



The similarity theory of free turbulent shear flows of viscoelastic fluids

Mateus C. Guimarães^{a,*}, Fernando T. Pinho^{b,c}, Carlos B. da Silva^a

^a IDMEC/LAETA, Instituto Superior Técnico, Universidade de Lisboa, Lisboa, Portugal

^b CEFT, Faculdade de Engenharia, Universidade do Porto, Porto, Portugal

^c ALiCE, Faculdade de Engenharia, Universidade do Porto, Porto, Portugal

ARTICLE INFO

Keywords:

Jets/wakes

Viscoelasticity

Turbulence theory

Turbulence simulation

ABSTRACT

A new theory is formulated for the description of the conformation state of the polymer chains in free turbulent shear flows of viscoelastic fluids. Using self-similarity arguments and new scaling relations for the turbulent flux of conformation tensor we show the existence of minimum and maximum solvent dissipation reduction asymptotes, and four different polymer deformation regimes. The similarities with the maximum drag reduction asymptote of turbulent pipe flow is discussed and new scaling laws are obtained for all components of the mean conformation tensor at each deformation regime. Analytical solutions for the self-similar transverse profiles of the conformation tensor components are also obtained, providing the complete solution for the mean flow problem at the far field. The analysis is developed for both planar jets and wakes and covers the two limits of shear flows, with large and small velocity differences, respectively. Comparisons of the new theoretical results with several direct numerical simulations employing the FENE-P rheological model show excellent agreement.

1. Introduction

Turbulent shear flows in the absence of solid walls, such as free turbulent jets and wakes, constitute a case of particular importance for the study of fluid turbulence. These flows have been subject to theoretical analyses since the early days of turbulence research (Prandtl 1925; Tollmien 1926; Schlichting 1930; Görtler 1942) [1–4] and the resulting theory has been documented in several textbooks of turbulence (Hinze 1959; Townsend 1976; Tennekes and Lumley 1972; Pope 2000) [5–8]. For incompressible flows of Newtonian fluids, the two-dimensional mean velocity and Reynolds stress components are the main objects of analysis and their downstream evolution is described by scaling laws obtained from self-similarity arguments and the assumption that the spreading of the shear layers is slow *i.e.*, the thin-shear layer approximation, invoked for high Reynolds number flows. The corresponding forms of the transverse profiles are typically obtained from the analytical solution of the momentum equation coupled with an eddy viscosity assumption.

However, when long chain polymer molecules are added to the Newtonian solvent the resulting fluid is viscoelastic and a complete description of the mean field problem requires the solution of additional entities like the mean conformation tensor, describing the elongation and orientation of the polymer chains, and the turbulent polymer stretching tensor associated with the flux of turbulent kinetic energy of the flow to elastic energy of the chains (Guimarães et al. 2020, 2022) [9,10].

Here we present a detailed theory for the conformation of the polymer chains in free turbulent shear flows with long-chain dilute polymer solutions. The theory is based on a similarity analysis of the equations governing the evolution of each component of the conformation tensor, which allows us to obtain several new results that provide a rich description of the elongation and orientation of the polymer chains. We show that the far field of high Weissenberg number turbulent shear flows is composed of four distinct sub-regions corresponding to different regimes of polymer deformation.

A summary of the four flow regions and polymer deformation regimes is displayed at figure Fig. 1. There is the near-field region, where either the flow is transitioning from laminar to turbulent or it is not yet fully developed, and the far-field fully turbulent region of interest in this analysis. In terms of viscoelastic effects on the flow dynamics, there is a highly elastic region encompassing the near field and the initial portion of the far field, and farther away, a low elasticity region where viscoelastic effects are milder [10]. When we consider the deformation of the polymer chains there is a highly-stretched and a nearly-coiled regime. The highly-stretched regime can be split into two sub-regimes, anisotropic (HSA) and nearly-isotropic (HSI), while the nearly-coiled regime contains a nearly-isotropic sub-regime (NCI) and the final region of decay (FD). This is a result of the decaying character of the flow strain rates, which are responsible for the deformation of the polymers. As will be demonstrated later, the normalized conformation

* Corresponding author.

E-mail address: mateus.carvalho@tecnico.ulisboa.pt (M.C. Guimarães).

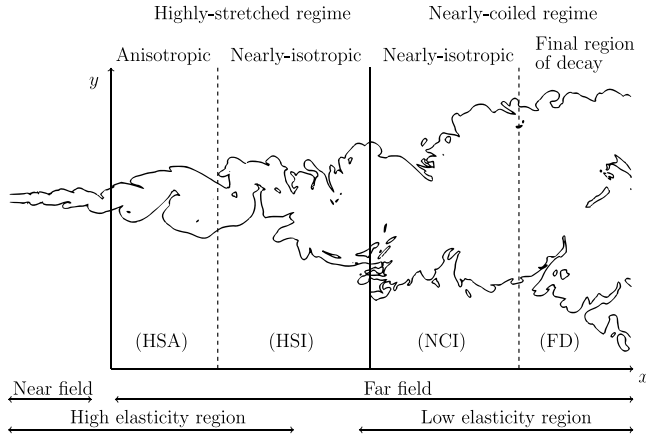


Fig. 1. Schematic diagram showing the different flow regions, at the bottom, and the corresponding polymer chain deformation regimes at the top. The diagram depicts the particular case of a jet with a high inlet Weissenberg number and a very long domain size in the streamwise direction, so that all different polymer deformation regimes are present. The scale is arbitrary.

tensor can be nearly-isotropic at both highly-stretched and nearly-coiled regimes because at the corresponding sub-regimes the stretching of the polymer chains is imposed predominately by intermediate and small scale fluctuating strains which are approximately isotropic.

The evolution of flow instabilities at the near-field region has been studied in [11–14], and also in Guimarães et al. (2023) [15], whereas the turbulent velocity and passive/active scalar statistics at the far-field were studied in Guimarães et al. (2020, 2022, 2022c) [9,10,16]. At the highly-stretched anisotropic regime (Fig. 1) the polymer structure is described by the scaling laws obtained in Guimarães et al. (2020, 2022) [9,10], to be briefly discussed later, and here the focus of the theory is on the three subsequent regimes.

In this work new scaling laws are obtained for each component and for the trace of the conformation tensor at the different deformation regimes. By complementing the governing equations with some eddy viscosity calculations for unclosed Newtonian terms, together with a dissipation law generalized for viscoelastic fluids and, by solving the resulting self-similar ordinary differential equations we are able to obtain the asymptotic solutions for the mean conformation tensor at $x \rightarrow \infty$, providing the complete solution of the mean field problem at this asymptotic limit, *i.e.* at the final region of decay. Additionally, we show the existence of minimum and maximum solvent dissipation reduction asymptotes and their relations with the obtained scaling laws. The similarities and differences to the maximum drag reduction asymptote of turbulent pipe and channel flows are also discussed.

All new theoretical results are validated by a large number of new DNS of spatially evolving turbulent planar jets and wakes employing the Finitely Extensible Non-Linear Elastic constitutive model closed with Peterlin's approximation (FENE-P) that use computational domains that are considerably larger than those used at Guimarães et al. (2020, 2022) [9,10] and that span a set of rheological and flow parameters that are also considerably larger than that presented before.

The governing equations and the numerical and physical parameters of the DNS are detailed at Section 2. Budgets of conformation tensor are discussed at Section 3 while the minimum and maximum *SDR* asymptotes and the resulting scaling for the turbulent polymer stretching tensor are derived at Section 4. Sections 5 and 6 present the self-similarity analysis of the equations that dictate the conformation state of the polymer chains, for turbulent planar wakes and jets, respectively, and the asymptotic solutions for the transverse profiles are shown in Section 7. A summary of the main results and conclusions are presented in Section 8.

To enhance the manuscript readability, several mathematical details are left to appendix sections, and Section 6, devoted to planar jets, only reports the results instead of discussing them in detail. The main ideas of the theory can be learned from Sections 4 and 5, the latter discussing in detail the wake flow, where we apply the framework summarized below.

1.1. General framework of the theory

The first steps are the choice of a rheological model that provides an evolution equation for the conformation tensor C , and the decomposition of the conformation tensor into mean and fluctuating components, \bar{C} and C' , respectively. Then, physical intuition is used to obtain scaling relations for each relevant term of the evolution equation of \bar{C} at the different polymer deformation regimes. After normalization of each term of the equation of \bar{C} , using the corresponding scaling relations, the distinguished limits of the equation are calculated, resulting in simplified equations that are the leading-order approximations of the general equation at different asymptotic regimes. Budgets of conformation tensor are then used to verify the accuracy of the approximations. Finally, mathematical inspection is used to analyse the possibility of self-similarity solutions at each regime.

Here we adopt the FENE-P rheological model and the classical Reynolds decomposition, *i.e.* $C = \bar{C} + C'$, where as usual the arithmetic mean is used to evaluate \bar{C} from C . However, the general framework summarized above, and elaborated at Section 4 and Section 5, can be applied to other rheological models, to flows with non-uniform polymer concentrations, or can be used with alternative turbulent decompositions of C , such as the geometric decomposition and averaging of C or the log-Euclidean averaging proposed recently by Hameduddin et al. (2018) [17] and Hameduddin and Zaki (2019) [18]. In Appendix E we provide comparisons between the different definitions of \bar{C} , *i.e.* arithmetic and log-Euclidean means, and show that our scaling laws are also able to describe \bar{C} when the log-Euclidean mean is used instead of the classical arithmetic mean.

A crucial assumption of the theory is the scaling law for the total dissipation rate of turbulent kinetic energy, and their asymptotic limits at high and low elasticity, discussed in detail in Section 4, the results of which are applied in the analysis of Section 5.

2. Direct numerical simulations

2.1. Governing equations and numerical method

The rheology of the polymer solutions is characterized by the FENE-P model developed by Bird et al. (1980) [19], but in a slightly modified form due to Sureshkumar et al. (1997) [20]. The momentum equation is

$$\frac{\partial \mathbf{u}}{\partial t} + \mathbf{u} \cdot \nabla \mathbf{u} = -\frac{1}{\rho} \nabla p + \nu^{[s]} \nabla^2 \mathbf{u} + \frac{1}{\rho} \nabla \cdot \boldsymbol{\sigma}^{[p]}, \quad (1)$$

where \mathbf{u} is the velocity vector and p is the pressure. The polymer stress tensor is

$$\boldsymbol{\sigma}^{[p]} = \frac{\rho \nu^{[p]}}{\tau_p} [f(C_{kk})C - I], \quad (2)$$

and the equation for the evolution of the conformation tensor C is given by

$$\frac{\partial C}{\partial t} + \mathbf{u} \cdot \nabla C = \nabla \mathbf{u}^T \cdot C + C \cdot \nabla \mathbf{u} - \frac{1}{\tau_p} [f(C_{kk})C - I]. \quad (3)$$

The Peterlin function used in the present work is given by $f(C_{kk}) \equiv (L^2 - 3)/(L^2 - C_{kk})$ and the fluid incompressibility condition is imposed by the continuity equation

$$\nabla \cdot \mathbf{u} = 0. \quad (4)$$

The polymer and solvent zero-shear kinematic viscosities are $\nu^{[p]}$ and $\nu^{[s]}$, respectively, τ_p is the polymer relaxation time, L is the maximum

Table 1
Physical and computational parameters of the simulations. For wakes, consider $L_x/d \times L_y/d \times L_z/d$ instead.

Flow type	Wi	Re	$1 - \beta$	L	Re_λ	$\frac{\Delta x}{\eta}$	$n_x \times n_y \times n_z$	$\frac{L_x}{h} \times \frac{L_y}{h} \times \frac{L_z}{h}$	Non-dimensional inlet noise
Jet	0.05	3500	0.20	100	162	1.9	1152 × 1024 × 128	40.5 × 36 × 4.5	0.1
	0.15	3500	0.20	100	145	2.0	1152 × 1024 × 128	40.5 × 36 × 4.5	0.1
	0.30	3500	0.20	100	146	2.0	1152 × 1152 × 144	40 × 40 × 5	0.1
	0.60	3500	0.20	100	153	1.9	1152 × 1152 × 144	40 × 40 × 5	0.1
	0.30	2500	0.20	100	146	2.0	960 × 768 × 88	50 × 40 × 4.6	0.15
	0.30	2500	0.02	100	138	2.0	960 × 768 × 88	50 × 40 × 4.6	0.15
	0.50	2500	0.02	100	150	2.0	960 × 768 × 88	50 × 40 × 4.6	0.15
	0.30	1500	0.20	100	104	1.8	704 × 576 × 64	48.9 × 40 × 4.5	0.15
	0.006	2000	0.20	100	125	1.7	896 × 768 × 96	42 × 36 × 4.5	0.15
	2	3500	0.02	100	205	2.5	576 × 576 × 128	20 × 20 × 4.5	0.15
	2	3500	0.20	100	260	2.5	576 × 576 × 128	20 × 20 × 4.5	0.15
	3	3500	0.01	100	185	2.6	576 × 576 × 128	20 × 20 × 4.5	0.15
	3	3500	0.02	100	208	2.4	576 × 576 × 128	20 × 20 × 4.5	0.15
	3	3500	0.10	100	300	2.4	576 × 576 × 128	20 × 20 × 4.5	0.15
	3	3500	0.20	100	311	2.3	576 × 576 × 128	20 × 20 × 4.5	0.15
	3	3500	0.02	200	316	2.4	576 × 576 × 128	20 × 20 × 4.5	0.15
	4	3500	0.01	100	188	2.6	576 × 576 × 128	20 × 20 × 4.5	0.15
	4	3500	0.02	100	219	2.4	576 × 576 × 128	20 × 20 × 4.5	0.15
	4	3500	0.20	100	350	2.4	576 × 576 × 128	20 × 20 × 4.5	0.15
	4	3500	0.02	200	281	2.8	576 × 576 × 128	20 × 20 × 4.5	0.15
5	3500	0.02	100	222	2.4	576 × 576 × 128	20 × 20 × 4.5	0.15	
4	2500	0.01	100	171	2.0	960 × 768 × 88	50 × 40 × 4.6	0.15	
4	2500	0.02	100	181	2.0	960 × 768 × 88	50 × 40 × 4.6	0.15	
4	2500	0.04	100	172	1.9	960 × 768 × 88	50 × 40 × 4.6	0.15	
4	2500	0.06	100	212	1.9	960 × 768 × 88	50 × 40 × 4.6	0.15	
5	2500	0.02	200	260	1.9	1408 × 1152 × 64	97.8 × 80 × 4.6	0.15	
Wake	0.0001	1500	0.20	100	60	3.4	2048 × 192 × 64	160 × 15 × 5	0.15
	0.0003	1500	0.20	100	61	3.4	1792 × 256 × 58	140 × 15 × 4.53	0.1
	0.005	4000	0.20	100	100	3.1	3456 × 576 × 144	120 × 20 × 5	0.1
	0.05	4000	0.20	100	114	2.8	3456 × 576 × 144	120 × 20 × 5	0.1
	0.15	4000	0.20	100	115	2.8	3456 × 576 × 144	120 × 20 × 5	0.1
	0.30	4000	0.20	100	115	2.8	3456 × 576 × 144	120 × 20 × 5	0.1
	0.30	4000	0.02	100	114	2.8	3456 × 576 × 144	120 × 20 × 5	0.1
	0.15	3000	0.20	100	102	3.2	2304 × 384 × 96	120 × 20 × 5	0.1
	0.15	1500	0.20	100	70	3.0	1536 × 256 × 64	120 × 20 × 5	0.1
	3	2000	0.02	200	107	1.6	4608 × 384 × 106	198 × 16.5 × 4.55	0.1
	5	2000	0.02	100	102	1.4	4608 × 384 × 106	198 × 16.5 × 4.55	0.1
	4	4000	0.01	100	166	2.6	2560 × 512 × 144	80 × 16 × 4.5	0.1
	4	4000	0.02	100	204	2.5	2560 × 512 × 144	80 × 16 × 4.5	0.1
	4	4000	0.04	100	217	2.4	2560 × 512 × 144	80 × 16 × 4.5	0.1
	4	4000	0.06	100	211	2.3	2560 × 512 × 144	80 × 16 × 4.5	0.1

length of the polymer dumbbell model normalized by its equilibrium size and ρ is the density of the fluid.

The momentum equation is solved with a highly accurate finite differences code that uses a combination of pseudo-spectral and 6th-order Compact schemes [21,22]. An explicit 3rd-order Runge–Kutta scheme is used for time-advancement [23] while the pressure–velocity coupling is treated with a fractional step method [24]. Inflow and non-reflective outflow boundary conditions are used at the two boundaries facing the flow direction. The equation for the conformation tensor is solved with the scheme proposed by Vaithianathan et al. (2006) [25], which is based on the shock-capturing method of Kurganov and Tadmor (2000) [26] and makes no use of any artificial numerical diffusion. This method can give first or second order accuracy for the advection term of the equation for C depending on the values of its eigenvalues. For the simulations presented here, it has been verified that second order accuracy is obtained for more than 98% of the points of the domain at all time steps. More details about the employed numerical methods and validation of our code can be found at Guimarães et al. (2020) [9].

2.2. Physical and computational parameters

A summary of the physical and numerical parameters of the DNS are given at Table 1. For planar jets with issuing velocity U_j and slot width h , the inlet Weissenberg number is $Wi = \tau_p U_j / h$ and the inlet Reynolds number is $Re = U_j h / \nu^{[s]}$. For planar wakes with free stream velocity U_∞ , inlet velocity deficit ΔU_0 , inlet momentum thickness θ and

solid body transverse length scale d , the inlet Weissenberg number is $Wi = \tau_p \Delta U_0 / d$ and the inlet Reynolds number is $Re = \Delta U_0 d / \nu^{[s]}$. The ratio of zero shear rate viscosities is

$$\beta = \frac{\nu^{[s]}}{\nu^{[s]} + \nu^{[p]}}. \quad (5)$$

For dilute solutions (β close to one) the polymer concentration is approximately proportional to $1 - \beta$. The number of grid points of the uniform computational mesh in each spatial direction is n_x , n_y and n_z , with corresponding domain sizes given by L_x , L_y and L_z . Here we consider long polymer chains ($L \gg 1$), semi-dilute ($1 - \beta = 0.20$ and 0.10) and dilute ($1 - \beta \lesssim 0.06$) polymer solutions.

A total of 41 DNS were performed, with rheological and flow parameters varying in the ranges given by $0.0001 \leq Wi \leq 5$, $1500 \leq Re \leq 4000$, $0.01 \leq 1 - \beta \leq 0.20$ and $100 \leq L \leq 200$. This large number of simulations allows us to validate the theory over a wide range of conditions. Additionally, in Appendix C we provide analytical expressions defining the domain of validity of each scaling law. They can be useful e.g. to assess the validity of each law when they have to be used in conditions that are outside the range of our simulations.

The local Reynolds number based on the root-mean-squared (rms) velocity $\sqrt{u'^2}$ and Taylor micro-scale λ is $Re_\lambda = \sqrt{u'^2} \lambda / \nu^{[s]}$, where $\lambda = (15 \nu^{[s]} u'^2 / \epsilon^{[s]})^{1/2}$ and $\epsilon^{[s]} = 2 \nu^{[s]} S'_{ij} S'_{ij}$ is the solvent mean viscous dissipation rate of turbulent kinetic energy ($S'_{ij} = (\partial u'_i / \partial x_j + \partial u'_j / \partial x_i) / 2$ is the fluctuating rate of strain tensor). The mesh resolution is quantified by the ratio between the grid spacing Δx and the Kolmogorov

length scale $\eta = (\nu^{[s]^3}/\epsilon^{[s]})^{1/4}$. In Table 1 we show values of Re_λ and $\Delta x/\eta$ that are characteristic of the far field region of the flow.

The details of the velocity and conformation field prescribed at the inlet boundary are described in detail in Guimarães et al. (2020; 2022) [9,10], for jets and wakes, respectively. The inlet velocity is based on a hyperbolic-tangent mean profile and a fluctuating component with a broadband white noise with a spectrum characteristic of isotropic turbulence. Here we use similar values for the inlet velocity parameters. For jets, the inverse of the normalized momentum thickness is $h/\theta = 30$ and the Strouhal number associated with the inlet noise spectrum peak is $St = f_{in}\theta/U_{conv} = 0.03$, where the convection velocity at the inlet is $U_{conv} = (U_J + U_\infty)/2$, with U_∞ here being a small jet co-flow velocity, the peak frequency of the inlet noise is $f_{in} = U_{conv}\kappa_p/(2\pi)$ and κ_p is the peak wave number. For wakes, the velocity gradient parameter is $d/\Phi = 60$ while $St = f_{in}\Phi/U_{conv} = 0.11$. The maximum amplitude values of the inlet noise, normalized by the mean velocity U_J or U_∞ of each simulation, are also indicated at Table 1. For the inlet conformation tensor we use the analytical solutions of the laminar Couette flow of FENE-P fluids derived by Pinho et al. (2008) [27], considering the local value of the velocity gradient at each grid point.

For turbulent jets we define the flow half width $\delta(x)$ as in Guimarães et al. (2020) [9] i.e. based on an integral of the normalized mean velocity profile: $\delta(x) = \int_0^\infty [\bar{u}(x, y)/U_c(x)] dy$. For wakes we adopt the classical definition, that is $\Delta\bar{u}(x, y) = \delta(x) = \Delta U(x)/2$, where the local mean velocity deficit is $\Delta\bar{u}(x, y) = U_\infty - \bar{u}(x, y)$ and $\Delta U(x) = \Delta\bar{u}(x, y = 0)$.

The scaling laws for the jet centreline mean velocity $U_c(x)$ and $\delta(x)$ are given by

$$\left[\frac{U_c(x)}{U_J}\right]^{-2} = A_{U_c} \left(\frac{x-x_0}{h}\right), \quad \frac{\delta(x)}{h} = A_\delta \left(\frac{x-x_0}{h}\right) \quad (6a,b)$$

while the scaling laws for the wake centreline mean velocity deficit $\Delta U(x) = U_\infty - \bar{u}(x, y = 0)$ and $\delta(x)$ are

$$\left[\frac{\Delta U(x)}{U_\infty}\right]^{-2} = A_{\Delta U} \left(\frac{x-x_0}{\theta}\right), \quad \left[\frac{\delta(x)}{\theta}\right]^2 = A_{\delta^2} \left(\frac{x-x_0}{\theta}\right) \quad (7a,b)$$

where x_0 is the virtual origin. The scaling law coefficients A_δ , A_{δ^2} , A_{U_c} and $A_{\Delta U}$ are typically obtained from an empirical fit of experimental and numerical data, and presently there is no theory that is able to calculate them from first principles, even for Newtonian flows. The curve-fitted values for the scaling laws coefficients for different flows follow the trends already reported and discussed in detail at Guimarães et al. (2020, 2022) [9,10].

To illustrate the simulations we show two-dimensional contours of instantaneous vorticity magnitude and polymer chain extension for turbulent jets and wakes, in Figs. 2 and 3, respectively. The flow structures have already been studied in detail in Guimarães et al. (2020, 2022) [9, 10]; the same trends have been observed in the new simulations performed here, using much bigger computational domains.

3. Budgets of mean conformation tensor

Budgets of the mean conformation tensor components are useful for identifying the physical mechanisms dictating the elongation and orientation of the polymer chains for cases involving different flow conditions and their description will be the focus of this section. Adopting the usual Reynolds decomposition and averaging, the equation governing the evolution of each non-zero component of the mean conformation tensor $\overline{C_{ij}}$ for a statistically steady flow is

$$\begin{aligned} \bar{u}_k \frac{\partial \overline{C_{ij}}}{\partial x_k} = & \left(\overline{C_{jk}} \frac{\partial \bar{u}_i}{\partial x_k} + \overline{C_{ik}} \frac{\partial \bar{u}_j}{\partial x_k} \right) - \overline{u'_k \frac{\partial c'_{ij}}{\partial x_k}} \\ & + \left(c'_{kj} \frac{\partial \bar{u}'_i}{\partial x_k} + c'_{ik} \frac{\partial \bar{u}'_j}{\partial x_k} \right) - \frac{\overline{\sigma_{ij}^{[p]}}}{\rho\nu^{[p]}} \end{aligned} \quad (8)$$

where an over-bar stands for the Reynolds average and a prime denotes the fluctuations with respect to the mean value (e.g. the instantaneous

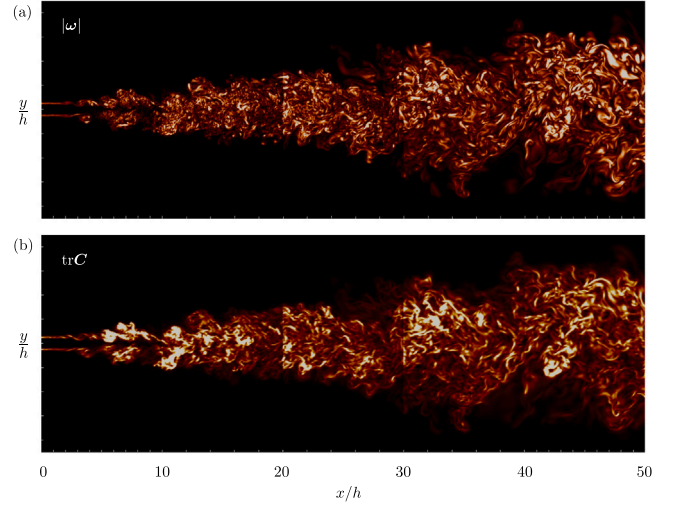


Fig. 2. Two dimensional contours of instantaneous vorticity modulus (a) and trace of conformation tensor (b) for a planar jet with $Wi = 0.5$, $Re = 2500$ and $1 - \beta = 0.02$. For clarity, the colourmap range is changed for every 10 units increment in x/h . Notice that the figures do not show the total extent of the domain in the vertical direction.

conformation tensor is $C_{ij} = \overline{C_{ij}} + c'_{ij}$). The mean polymer stress is calculated from its definition i.e. $\overline{\sigma_{ij}^{[p]}} = \rho\nu^{[p]}(f(C_{kk})C_{ij} - \delta_{ij})/\tau_p$. The mean advection of $\overline{C_{ij}}$ is given by $\bar{u}_k \partial \overline{C_{ij}}/\partial x_k$, mean polymer chain stretching is $\overline{C_{jk}} \partial \bar{u}_i/\partial x_k + \overline{C_{ik}} \partial \bar{u}_j/\partial x_k$ while turbulent advection is given by $\overline{u'_k \partial c'_{ij}/\partial x_k}$ and $\overline{c'_{kj} \partial \bar{u}'_i/\partial x_k} + \overline{c'_{ik} \partial \bar{u}'_j/\partial x_k}$ is the turbulent stretching term. The mean chain relaxation term is $\overline{\sigma_{ij}^{[p]}}/(\rho\nu^{[p]})$. The turbulent stretching tensor is very important and its trace appears in the transport equation for the trace $\overline{C_{ii}}$ and also for the turbulent kinetic energy κ , but with opposite signs at each equation, so that it represents flux between the turbulent kinetic energy of the flow and mean elastic energy of the polymers (which is proportional to $\overline{C_{ii}}$).

The analysis of the four different regimes summarized in Fig. 1 is supported by the budgets of $\overline{C_{xy}}$ and $\overline{C_{xx}}$, presented here for turbulent wakes. The budgets of the remaining $\overline{C_{ij}}$ components are shown in Appendix A. The results for jets are qualitatively similar, and are also shown in Appendix A.

Considering first the $\overline{C_{xy}}$ component at the highly-stretched anisotropic regime (HSA), most terms of the equation are important except for $\overline{C_{xx}} \partial \bar{v}/\partial x$ and $-\bar{v} \partial \overline{C_{xy}}/\partial y$, which are negligible everywhere (Fig. 4a). The $\overline{C_{xy}}$ component has opposite signs for jets and wakes because $\partial \bar{u}/\partial y$ is negative for jets and positive for wakes (for $y/\delta > 0$) and so the sign is reversed for jets. Nonetheless, the physical mechanism is the same: increasing of $\pm \overline{C_{xy}}$ is caused predominantly by mean stretching $\overline{C_{yy}} \partial \bar{u}/\partial y$, while mean flow advection $-\bar{u} \partial \overline{C_{xy}}/\partial x$ gives a small contribution at $0 \lesssim y/\delta \lesssim 1.5$. Mean relaxation $-\overline{\sigma_{xy}^{[p]}}/(\rho\nu^{[p]})$ and turbulent stretching $\overline{c'_{ky} \partial \bar{u}'_i/\partial x_k} + \overline{c'_{xk} \partial \bar{v}'_i/\partial x_k}$ are responsible for dissipating $\pm \overline{C_{xy}}$. The turbulent advection term $\overline{u'_k \partial c'_{xy}/\partial x_k}$ is the only term that changes sign, advecting $\pm \overline{C_{xy}}$ from the shear layer region ($y/\delta \approx 0.8$), where $\pm \overline{C_{xy}}$ is maximum, to regions nearby the jet/wake irrotational boundary. For the remaining deformation regimes the dynamics of $\overline{C_{xy}}$ becomes progressively simpler. At the highly-stretched nearly-isotropic regime the turbulent advection term $\overline{u'_k \partial c'_{xy}/\partial x_k}$ becomes negligibly small (Fig. 4b). For the nearly-coiled regimes there is a tendency for approaching a state where a balance between mean stretching $\overline{C_{yy}} \partial \bar{u}/\partial y$ and relaxation $-\overline{\sigma_{xy}^{[p]}}/(\rho\nu^{[p]})$ is observed (Fig. 4c,d).

The budgets for the normal $\overline{C_{ij}}$ components at the highly-stretched anisotropic regime are qualitatively similar to that for $\overline{C_{xy}}$ described above (Fig. 4e). The main difference is that stretching by the mean velocity gradient $\overline{C_{jk}} \partial \bar{u}_i/\partial x_k + \overline{C_{ik}} \partial \bar{u}_j/\partial x_k$ is zero for the $ij = zz$ component

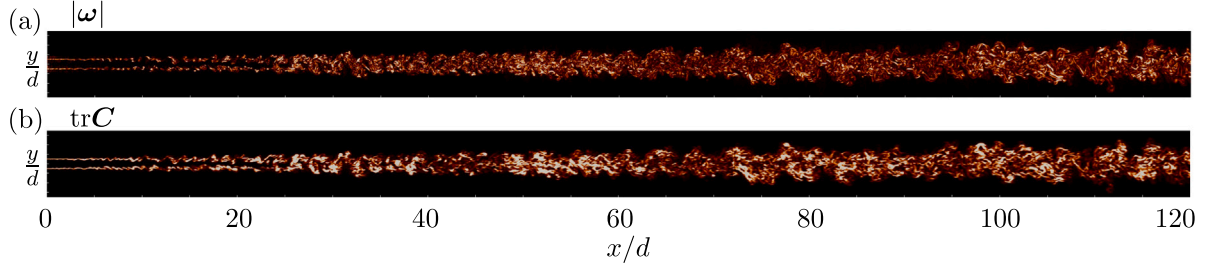


Fig. 3. Two dimensional contours of instantaneous vorticity modulus (a) and trace of conformation tensor (b) for planar wakes with $Wi = 0.3$, $Re = 4000$ and $1 - \beta = 0.02$. For clarity, the colourmap range is changed for every 24 units increment in x/d . Notice that the figures do not show the total extent of the domain in the vertical direction.

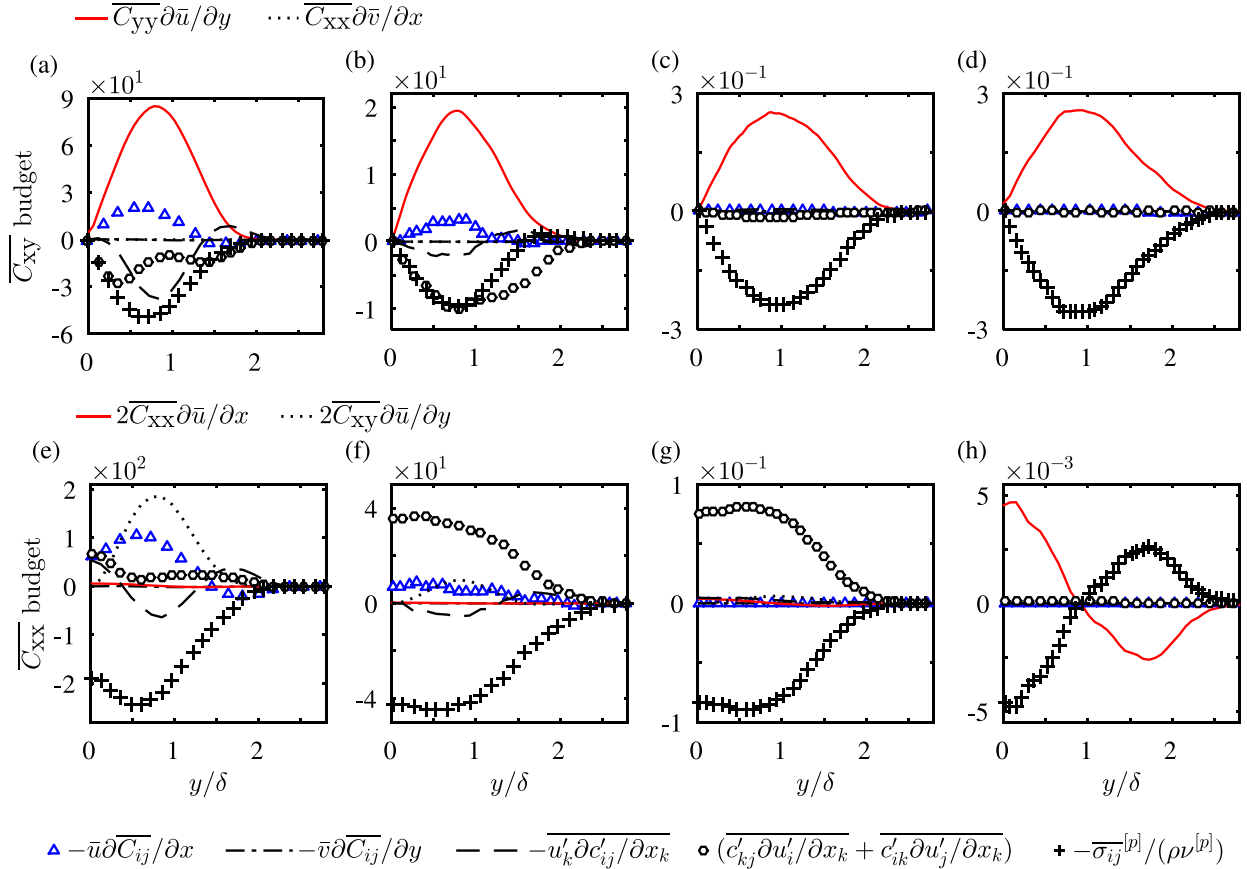


Fig. 4. Budgets of \overline{C}_{xy} (a-d) and \overline{C}_{xx} (e-h) for wakes at different regimes of polymer chain deformation: (a,e) highly-stretched anisotropic, (b,f) highly-stretched nearly-isotropic, (c,g) nearly-coiled nearly-isotropic and (d,h) final region of decay. All quantities have been made non-dimensional using U_{∞} and d . Flow conditions are: (a) and (e) $Re = 2000$, $Wi = 4$, $1 - \beta = 0.10$, $L = 100$, $x/d = 70$; (b) and (f) $Re = 2000$, $Wi = 3$, $1 - \beta = 0.02$, $L = 200$, $x/d = 180$; (c) and (g) $Re = 4000$, $Wi = 0.05$, $1 - \beta = 0.20$, $L = 100$, $x/d = 110$; (d) and (h) $Re = 1500$, $Wi = 0.0001$, $1 - \beta = 0.20$, $L = 100$, $x/d = 110$.

(due the symmetry of the mean flow) and is relatively small for the $ij = yy$ component, giving an important contribution predominantly for \overline{C}_{xx} . This is a consequence of the slender character of the shear layer (small spreading rates) and results in \overline{C}_{xx} values that are larger than \overline{C}_{yy} and \overline{C}_{zz} at the highly-stretched anisotropic regime. How much larger depends on flow and rheological parameters, but for the cases considered here it can be up to one order of magnitude larger—this was also reported in our previous works [9,10]. For the two nearly-isotropic regimes, highly stretched (HSI) and nearly-coiled (NCI), the flow attains a state where turbulent stretching $c'_{kj} \partial u'_i / \partial x_k + c'_{ik} \partial u'_j / \partial x_k$ is approximately balanced by mean relaxation $\overline{\sigma}_{ij}^{[p]} / (\rho \nu^{[p]})$ (Fig. 4f,g), as in the case of homogeneous isotropic turbulence, and indeed this explains the nearly isotropic centreline \overline{C}_{ij} values observed for these flow regimes. This is in contrast with the behaviour described above

for \overline{C}_{xy} , but at these flow regimes the normal components of \overline{C}_{ij} are much larger than the shear component.

Finally, at the final region of decay (FD) the mean stretching terms in the equations for \overline{C}_{xx} and \overline{C}_{yy} , i.e. $2\overline{C}_{xx} \partial \bar{u} / \partial x$ and $2\overline{C}_{yy} \partial \bar{v} / \partial y$ grow to become the dominant terms of the equations while the turbulent stretching terms become negligibly small (Fig. 4h). Interestingly, these mean stretching terms for \overline{C}_{xx} and \overline{C}_{yy} have opposite signs due to the incompressibility condition $\partial \bar{u} / \partial x = -\partial \bar{v} / \partial y$ and the nearly-coiled state of the polymer chains ($\overline{C}_{xx} \approx \overline{C}_{yy} \approx 1$) so that they cancel out when the ij indexes are contracted to obtain the equation for the trace \overline{C}_{ii} , meaning that the very small elongations at the final region of decay are dictated purely by the fluctuating strain rates as in isotropic turbulence. The budget of the trace \overline{C}_{ii} is similar to the budget of \overline{C}_{zz} , shown in Appendix A.

4. Maximum and minimum SDR asymptotes and the scaling of the turbulent polymer stretching tensor

Here we show the existence of maximum and minimum SDR asymptotes and develop expressions for the scaling of the turbulent stretching term of the \overline{C}_{ij} equation (normal components and trace) that will be crucial in the derivation of the scaling laws. These expressions will make use of the following scaling for the total (solvent plus polymer) dissipation rate of turbulent kinetic energy

$$\varepsilon^{[p]} + \varepsilon^{[s]} \sim \frac{\kappa^{3/2}}{\delta} \sim \frac{u'^3}{\delta}, \quad (9)$$

where $\kappa = (\overline{u'^2} + \overline{v'^2} + \overline{w'^2})/2$ and $u' \sim \sqrt{\kappa}$ is the turbulent velocity scale. This hypothesis is similar to the classical dissipation law for Newtonian fluids but the total dissipation appears in place of the solvent dissipation. It has already been observed for homogeneous and isotropic turbulence of viscoelastic FENE-P fluids [28,29] and can be very useful to describe free shear layers too, as will be demonstrated later.

This extended dissipation law will be used at both the highly-stretched and nearly-coiled regimes of polymer deformation. The turbulent velocity scale u' is different for jets and wakes and so the final forms of the $c'_{ij}\partial u'_i/\partial x_j$ scaling for each flow configuration will be presented only later at Sections 5 and 6.

The highly-stretched anisotropic and nearly-isotropic sub-regimes are dealt with at Section 4.1 whereas the nearly-coiled regimes, nearly-isotropic and final region of decay, are considered in Section 4.2. In fact, the maximum and minimum SDR asymptotes appear predominantly at the highly-stretched anisotropic and final region of decay, respectively, but the resulting scaling relations for the turbulent stretching tensor are valid also for the other sub-regimes (as shown at later sections).

We expect that the expressions shown in this section are general and can be applied to other turbulent flow configurations such as free shear layers in the axisymmetric configuration, decaying turbulence behind a grid and possibly some region of a flat plate boundary layer, provided adequate turbulent velocity and length scales are specified. They can also be useful in the derivation of RANS and LES closure models for the turbulent polymer stretching term, as any closure equation should at least capture the correct scaling behaviour at the limiting cases of high and low elasticity. Finally, we note that no particular rheological model is adopted in the derivation of the minimum and maximum SDR asymptotes.

4.1. Highly-stretched regimes

In this regime we use the following hypothesis

$$\varepsilon^{[p]} + \varepsilon^{[s]} \sim \varepsilon^{[p]}, \quad (10)$$

which states that the turbulent kinetic energy of the flow in the highly elastic regime, where the polymer chains are very stretched, is dissipated mainly by the polymers so that the total dissipation is proportional to $\varepsilon^{[p]}$. When the hypothesis is introduced in the definition of SDR , which is given by

$$SDR = \frac{\varepsilon^{[p]}}{\varepsilon^{[p]} + \varepsilon^{[s]}}, \quad (11)$$

we obtain the following scaling law

$$SDR = \tilde{A}_{SDR}, \quad (12)$$

where a scaling factor \tilde{A}_{SDR} close to one has been introduced. Eq. (12) indicates that in the highly elastic regime SDR is a constant independent of x , and possibly also independent of the inlet and rheological parameters Wi , Re , $1 - \beta$ and L , if the constant \tilde{A}_{SDR} is universal. To validate this result, the streamwise evolution of SDR is shown at Fig. 5 for turbulent jets and wakes with different combinations of inlet and

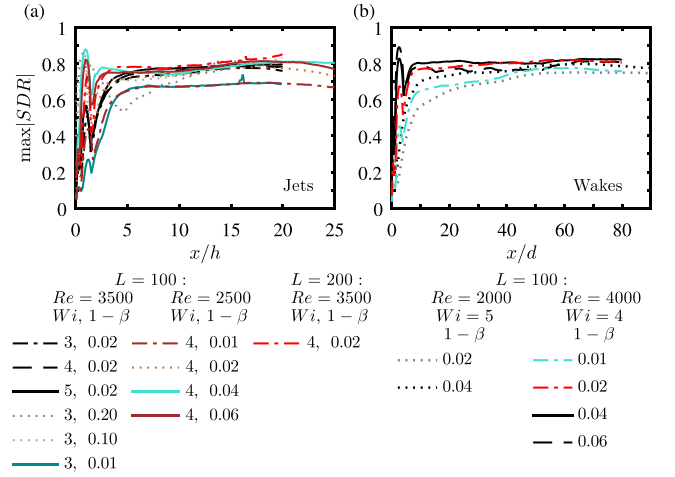


Fig. 5. Streamwise evolution of $\max[|\varepsilon^{[p]}|/(\varepsilon^{[s]} + |\varepsilon^{[p]}|)]$ at highly elastic regime for jets (a) and wakes (b), showing the maximum SDR asymptote.

rheological parameters, but always with $Wi \geq 3$, i.e. flows with high elasticity. After the initial transition region of the flow SDR attains a plateau, confirming that SDR is independent of x at the high elasticity portion of the far field, as predicted by Eq. (12). For large Re , the value of the plateau is approximately independent of Re , Wi and L . An initial increase in the polymer concentration parameter $1 - \beta$ from 0.01 to 0.02 also increases the plateau value of SDR , however from that point onwards it is clear that no more solvent dissipation reduction can be obtained from an increase in the polymer concentration and the flow has reached an asymptotic state where viscoelastic effects have saturated. SDR becomes invariant to $1 - \beta$ in this asymptotic regime. The value of this maximum SDR asymptote is given by $\tilde{A}_{SDR} = 0.78 \pm 0.03$, for both jets and wakes. The wakes with $Re = 2000$ show values of SDR that are smaller than the maximum SDR asymptote, and the values of \tilde{A}_{SDR} for different flow conditions are more scattered, indicating that for these cases Re is not sufficiently high for \tilde{A}_{SDR} to be universal. Nevertheless, \tilde{A}_{SDR} is always independent of x at the high elasticity regime, even for these cases with a lower Re .

The features of the maximum solvent dissipation reduction asymptote discussed above are very similar to those of the maximum drag reduction asymptote of turbulent pipe and channel flows, suggesting that the fundamental explanation for the existence of these asymptotes does not involve the presence of solid boundaries.

When the inlet Wi or local Deborah number $De (= \tau_p U_c / \delta$ for jets and $\tau_p \Delta U / \delta$ for wakes) are not sufficiently high, the maximum SDR asymptote is not observed, and the value of SDR will be in the range between the maximum and minimum asymptotes. The minimum SDR asymptote, discussed in the next section, is observed when the inlet Wi is not high enough to stretch the polymers significantly and the polymers will be in the nearly-coiled regime.

Combining Eq. (10) with the extended dissipation law (9) leads to $\varepsilon^{[p]} \sim u'^3 / \delta$. The scaling of the turbulent polymer stretching term is obtained from a scaling of $\varepsilon^{[p]}$ that is based on its definition i.e. considering the relation given by $f(c_{nn} + 3)c'_{ik}\partial u'_i/\partial x_k \sim \tau_p \varepsilon^{[p]} / \nu^{[p]}$, where $c_{ii} = \max[\overline{C}_{ii} - 3]$ so that $f(\max[\overline{C}_{ii}]) = f(c_{nn} + 3)$ i.e., henceforth we use $c_{ij}(x)$ (lower case without the fluctuation exponent) to denote characteristic values of the conformation tensor. Notice that we are using the same definition of the Peterlin function that has been adopted for our DNS computations. Combining these expressions we obtain the scaling of the turbulent stretching term at the highly-stretched regimes:

$$c'_{ij} \frac{\partial u'_i}{\partial x_j} \sim \frac{\tau_p u'^3}{\nu^{[p]} f(c_{nn} + 3) \delta}. \quad (13)$$

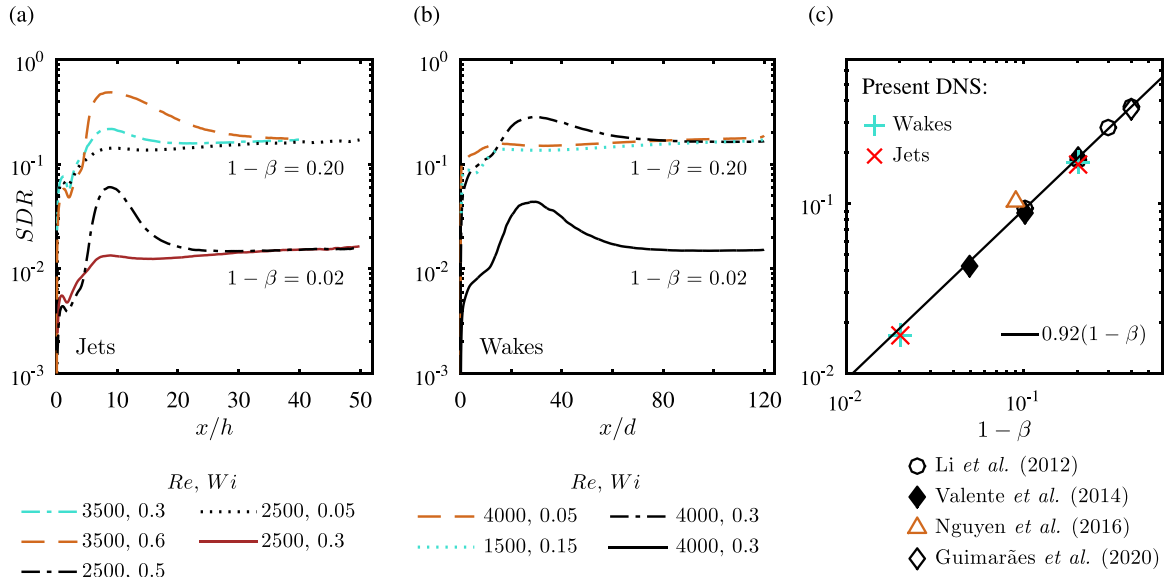


Fig. 6. Streamwise evolution of SDR for jets (a) and wakes (b) and far field plateau values against the concentration parameter $1 - \beta$ showing the minimum SDR asymptote (c).

4.2. Nearly-coiled regimes

At the nearly coiled regimes the local Deborah number $De(x)$ is low, which leads us to propose the following scaling hypothesis for the total (solvent plus polymer) dissipation rate

$$2\nu^{[s]}\overline{S' : S'} + \frac{\sigma'^{[p]} : \nabla\mathbf{u}'}{\rho} \sim 2(\nu^{[s]} + \nu^{[p]})\overline{S' : S'}. \quad (14)$$

The hypothesis states that for low $De(x)$ elasticity plays a weaker role on the averaged flow dynamics and energy cascade mechanism, merely introducing an extra dissipation of turbulent kinetic energy with a nearly (pseudo) viscous character, and a Newtonian behaviour is recovered with the total kinematic viscosity $\nu^{[s]} + \nu^{[p]}$ [28,29]. Using the definitions of $\varepsilon^{[s]}$, $\varepsilon^{[p]}$ and β , Eq. (14) can be written as

$$\varepsilon^{[s]} + \varepsilon^{[p]} \sim \frac{\varepsilon^{[s]}}{\beta}. \quad (15)$$

Isolating $\varepsilon^{[p]}$ and inserting the result in the definition of the solvent dissipation reduction parameter $SDR = \varepsilon^{[p]} / (\varepsilon^{[p]} + \varepsilon^{[s]})$ leads to $SDR \sim (1 - \beta)$, which after the introduction of a scaling factor A_{SDR} gives

$$SDR = A_{SDR}(1 - \beta). \quad (16)$$

The scaling relation given by Eq. (16) indicates that when the local Deborah number is low SDR is independent of x , and possibly of Wi and Re also, depending if A_{SDR} is universal, and varies linearly with the polymer concentration, which is proportional to $1 - \beta$. It is interesting to compare this law with Eq. (12) for the highly elastic regime, where we found that SDR is independent of the polymer concentration, at least for very dilute solutions at sufficiently high Re .

The results of our simulations indicate that at both nearly-coiled regimes SDR attains a plateau for large x/h or x/d , which is invariant with respect to Re or Wi and depends only on $1 - \beta$. This is shown at Figs. 6a,b, where it can also be seen that the plateau is reached further downstream as the inlet Wi is increased. The plateau values have been plotted against $1 - \beta$ at Fig. 6c, which also includes data from homogeneous isotropic turbulence (HIT) DNS at low De , taken from the literature [9,28,30,31]. It can be seen that Eq. (16) gives a good fit to the data with $A_{SDR} = 0.92$ indicating that Eqs. (15) and (16) can indeed capture the correct scaling relation. Thus, this scaling law defines the minimum possible value of SDR parameter for a flow with a given polymer concentration.

Isolating $\varepsilon^{[p]}$ in (15) and using $\varepsilon^{[p]} = 2\nu^{[p]}\overline{c'_{ki}\partial u'_i/\partial x_k}/\tau_p$, which is an exact relation for the Oldroyd-B fluid and an accurate approximation

for the FENE-P fluid in the particular case where the long chain polymers are in the nearly-coiled state and so $f(\overline{C_{kk}})$ is close to unity, will lead to

$$c'_{ij}\frac{\partial u'_i}{\partial x_j} \sim \frac{\tau_p}{\nu^{[s]}}\varepsilon^{[s]}. \quad (17)$$

Combining expression (17) with (15) and the extended dissipation law given by (9) we obtain the scaling of the turbulent stretching term at the nearly-coiled regimes

$$c'_{ij}\frac{\partial u'_i}{\partial x_j} \sim \frac{\beta\tau_p u'^3}{\nu^{[s]}\delta}. \quad (18)$$

5. Similarity laws of the conformation tensor: planar wake

It is instructive to do some preliminary considerations that are useful for the derivation of the $c_{ij}(x)$ scaling laws at the different polymer deformation regimes. The turbulent velocity scale of the planar wake is given by [10]

$$u' \sim \sqrt{\frac{\Delta U U_\infty}{2\delta} \frac{d\delta^2}{dx}}. \quad (19)$$

The momentum integral constraint of viscoelastic turbulent planar wakes is $d[\Delta U(x)\delta(x)]/dx = 0$ [10]. The momentum thickness Reynolds number $Re_\theta = U_\infty\theta/\nu^{[s]}$ is high and the non-dimensional spreading rate coefficient $A_{\delta^2} = (d\delta^2/dx)/\theta$ is small. Also small is the non-dimensional velocity deficit $\Delta U(x)/U_\infty$, while for dilute polymer solutions the parameter $\beta/(1 - \beta)$ is large. This flow condition will be considered at both highly-stretched and nearly-coiled regimes and, together with the limit relations that are specific to each regime, i.e. very large $c_{ij}(x)$ at the highly-stretched regime and very small $c_{ij}(x)$ at the nearly-coiled regime, they allow several simplifications of the governing equations.

The scaling laws at the highly-stretched nearly-isotropic regime are presented in Section 5.1, at the nearly-coiled nearly-isotropic regime in Section 5.2 and at the final region of decay in Section 5.3. To enhance the manuscript readability, some details of the derivation are omitted here and shown only in Appendix B. As mentioned in the Introduction, the theory of the highly-stretched anisotropic regime has been formulated at Guimarães (2020, 2022) [9,10] and thus will not be shown here, only the final results will be briefly discussed at the conclusions section.

5.1. Highly-stretched nearly-isotropic regime

The balance equations for \overline{C}_{ij} at the highly-stretched nearly-isotropic regime are given by

$$\overline{C}_{yy} \frac{\partial \overline{u}}{\partial y} + c'_{xk} \frac{\partial v'}{\partial x_k} + c'_{yk} \frac{\partial u'}{\partial x_k} = \frac{\overline{\sigma}_{xy}^{[p]}}{\rho v^{[p]}}, \quad (20)$$

for the shear \overline{C}_{xy} component and

$$2c'_{ik} \frac{\partial u'_j}{\partial x_k} = \frac{\overline{\sigma}_{ij}^{[p]}}{\rho v^{[p]}}, \quad (21)$$

for the normal components and trace of \overline{C}_{ij} . In Appendix B we show that the system described by the equations above is the leading order approximation of the general Eq. (8) when $c_{ij}(x)$ is large. The accuracy of the approximation can be evaluated from the budgets of \overline{C}_{ij} presented in Section 3 (Fig. 4b,f). To obtain the scaling laws of \overline{C}_{ij} we consider the following self-similarity relations

$$\frac{\Delta \overline{u}}{\Delta U} = \psi \left(\frac{y}{\delta} \right), \quad (22)$$

$$\frac{\overline{C}_{ij} - \delta_{ij}}{c_{ij}} = g_{ij} \left(\frac{y}{\delta} \right), \quad (23)$$

$$\frac{\overline{\sigma}_{ij}^{[p]}}{f(c_{nn} + 3)\rho v^{[p]}c_{ij}/\tau_p} = \sigma_{ij} \left(\frac{y}{\delta} \right), \quad (24)$$

$$\frac{2\zeta f(c_{nn} + 3)c'_{ik} \partial u'_j / \partial x_k}{[\beta/(1-\beta)]DeRe_\theta A_\delta^{5/4} A_{\Delta U}^{1/4} \Delta U / \delta} = N_{ij} \left(\frac{y}{\delta} \right), \quad (25)$$

$$\frac{c'_{xk} \partial v' / \partial x_k + c'_{yk} \partial u' / \partial x_k}{f(c_{nn} + 3)c_{xy} u^* / r^*} = N_{xy} \left(\frac{y}{\delta} \right), \quad (26)$$

where Eqs. (23) and (24) are for all normal and shear components, without summation on repeated ij indexes, and also for the trace but with a notation that avoids four repeated indexes on the same term. Eq. (25) is for the normal components and trace. $\Delta \overline{u}(x, y) = U_\infty - \overline{u}(x, y)$ is the local velocity difference. The characteristic scales $c_{ij}(x)$ are taken from the values of $\overline{C}_{ij} - \delta_{ij}$ at the y position where $|\overline{C}_{ij} - \delta_{ij}|$ is maximum, for both shear and normal components *i.e.*

$$c_{ij}(x) = \max |\overline{C}_{ij}(x, y) - \delta_{ij}|, \quad (27)$$

where as before $\overline{C}_{ij}(x, y)$ is the mean conformation tensor.

All variables appearing on the numerator at the l.h.s. of Eqs. (22)–(26) are functions of both x and y , while the corresponding characteristic scales, *i.e.* those variables appearing on the denominator, are functions of x only. At times, we shall explicitly show the x dependency of those quantities, for completeness, but often we will omit it, for compactness and clarity.

The validity of the self-similarity relations (22)–(26) is readily verified at Figs. 7 and 8 showing that the transverse profiles taken at different x stations collapse onto a single curve, for each quantity, when normalized according to Eqs. (22)–(26). The normalized mean velocity deficit is also self-similar and is insensitive to the polymers at the far field, as shown by Guimarães et al. (2022). The $\psi(y/\delta)$ curve is shown in that earlier paper, and also at Section 5.2 of the present manuscript.

The scaling for the turbulent polymer stretching components that appears in expression (25) has been obtained from Eqs. (13) and (19). The coefficient $\zeta = 2^{3/2}$ for the trace, and stems from the factor 2 that appears in Eq. (19), and for each normal components we use $\zeta = 3 \times 2^{3/2}$ *i.e.* the scale for the trace is three times larger than the scale of each normal component, as it should be. For the shear component of the turbulent polymer stretching tensor we rely on the Lumley scales of velocity u^* and length r^* , which are related to each other by the polymer relaxation time $r^*/u^* = \tau_p$, and account well for the correlation between the fluctuating velocity gradient and conformation tensors, as explained in our previous works [9,10]. In fact, the Lumley scales

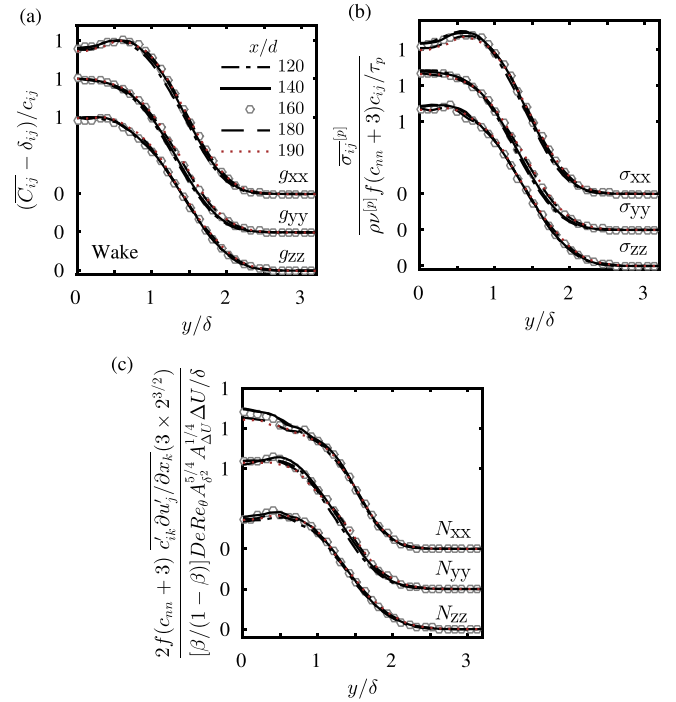


Fig. 7. Transverse profiles at different x/d stations normalized according to the proposed theory at the highly-stretched nearly-isotropic regime: normal components of (a) g_{ij} , (b) σ_{ij} and (c) N_{ij} , for the wake with $Wi = 5$, $Re = 2000$, $1 - \beta = 0.02$ and $L = 100$.

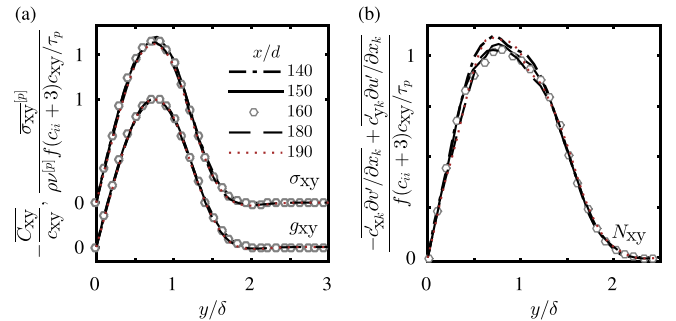


Fig. 8. Transverse profiles of shear components of g_{ij} and σ_{ij} (a) and N_{ij} (b) at the highly-stretched nearly-isotropic regime shown with similarity coordinates for the wake with $Wi = 5$, $Re = 2000$, $1 - \beta = 0.02$ and $L = 100$.

can also be used to formulate a scaling for the normal components and trace of the turbulent polymer stretching tensor, but the resulting self-similar equations are not useful for the derivation of the $c_{ij}(x)$ normal components and trace (not shown for brevity). The Peterlin function in Eq. (26) was introduced after an inspection of the resulting self-similarity equation of \overline{C}_{xy} .

Inserting Eqs. (22)–(26) into (20) and (21), performing some simple algebraic manipulations and considering the limit conditions discussed at the beginning of the section leads to the self-similarity equations

$$-\frac{Dec_{yy}}{f(c_{nn} + 3)c_{xy}} \left\{ g_{yy} \frac{d\psi}{d\xi} \right\} = \left\{ N_{xy} \right\} - \left\{ \sigma_{xy} \right\} \quad (28)$$

for the shear component \overline{C}_{xy} and

$$\frac{\beta De^2 Re_\theta}{(1-\beta)\zeta f(c_{nn} + 3)^2 c_{ij}} A_\delta^{5/4} A_{\Delta U}^{1/4} \left\{ N_{ij} \right\} = \left\{ \sigma_{ij} \right\} \quad (29)$$

for the normal components and trace (no summation on repeated ij indexes), where $\xi = y/\delta$. Given the self-similarity of $N_{ij}(\xi)$ and $\sigma_{ij}(\xi)$,

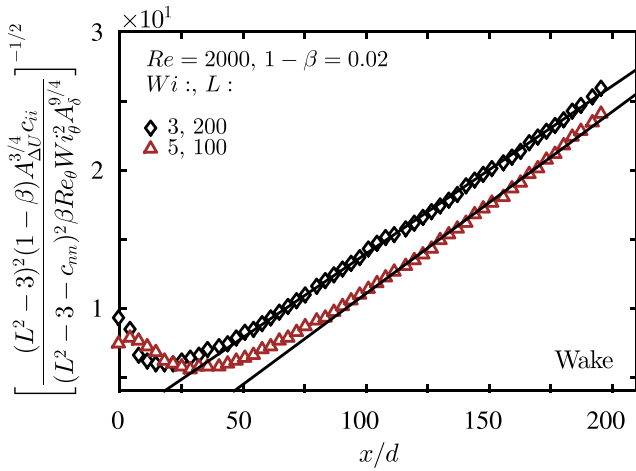


Fig. 9. Streamwise evolution of the normalized trace $c_{ii}(x)$ compared to the theory for turbulent wakes at the highly-stretched nearly-isotropic regime. Solid curves are straight line fits to the DNS data. Vertical shifts are applied for clarity. From top to bottom curves, the shifts are equal to 3 (black diamonds) and 0 (brown triangles).

the l.h.s. of Eq. (29) is a function of both x and ξ , while the r.h.s. is a function of ξ only. The only possibility where this condition is satisfied for all values of ξ is when

$$\frac{\beta De^2 Re_{\theta}}{(1-\beta)\zeta f(c_{nn}+3)^2 c_{ij}} A_{\delta}^{\frac{5}{4}} A_{\Delta U}^{\frac{1}{4}} \sim 1, \quad (30)$$

which after the substitution of the scaling laws for $\delta(x)$ and $\Delta U(x)$ in the definition of $De(x)$ and some rearrangement leads to the scaling law for the trace and normal components of the mean conformation tensor at the highly-stretched nearly-isotropic regime

$$\left\{ \frac{(L^2 - 3)^2 (1 - \beta) A_{\Delta U}^{3/4} c_{ij}(x)}{[L^2 - 3 - c_{nn}(x)]^2 \beta W i_{\theta}^2 Re_{\theta} A_{\delta}^{9/4}} \right\}^{-1/2} = \bar{A}_{c_{ij}} \left(\frac{x - x_0}{\theta} \right), \quad (31)$$

where $\bar{A}_{c_{ij}}$ are scaling law coefficients, x_0 is the virtual origin (the constant ζ is absorbed by $\bar{A}_{c_{ij}}$) and $W i_{\theta} = \tau_p U_{\infty} / \theta$. Using similar arguments for Eq. (28), a self-similar development is obtained provided $Dec_{yy} / [f(c_{nn} + 3)c_{xy}] \sim 1$, which will lead to the following scaling law for $c_{xy}(x)$ after the introduction of the scaling laws for $De(x)$ and $c_{yy}(x)$ and a scaling parameter $\bar{A}_{c_{xy}}$

$$\left\{ \frac{(L^2 - 3)^3 (1 - \beta) A_{\Delta U}^{1/4} A_{\delta}^{5/4} c_{xy}(x)}{[L^2 - 3 - c_{nn}(x)]^3 \beta W i_{\theta}^3 Re_{\theta}} \right\}^{-1/3} = \bar{A}_{c_{xy}} \left(\frac{x - x_0}{\theta} \right). \quad (32)$$

Considering Eq. (31) for the trace, isolating $c_{ii}(x)$ by solving the resulting second order algebraic equation for $c_{ii}(x)$ and calculating the limit $W i_{\theta}^2 Re_{\theta} \rightarrow \infty$ gives $c_{ii}(x) = \max\{C_{ii} - 3\} \rightarrow L^2 - 3$, which is the expected behaviour for polymer chains with maximum extensibility length given by L . This asymptotic value is also pertinent for the highly-stretched anisotropic regime, as discussed later at Section 8. The validity of the scaling laws is confirmed in Figs. 9 and 10. Because $c_{xx}(x)$, $c_{yy}(x)$, $c_{zz}(x)$ and trace $c_{ii}(x)$ follow the same scaling law at this particular deformation regime, the resulting figures for the different normal components are very similar except near the inlet of the computational domain, and thus only the $c_{xy}(x)$ component and trace $c_{ii}(x)$ are shown.

The values of the scaling law coefficients $\bar{A}_{c_{ij}}$ introduced here for the highly stretched regime, and later for the nearly-coiled regimes, are obtained for each case from a curve fitting of the DNS data, similarly to the procedure that is typically adopted in the classical theory of Newtonian turbulent flows to obtain A_{δ^2} , A_{δ} , A_{U_c} and $A_{\Delta U}$. In normalized units such as those of Figs. 9 and 10, corresponding to Eqs. (31) and (32), respectively, they represent the slopes of the straight lines that best fits the DNS data at each regime.

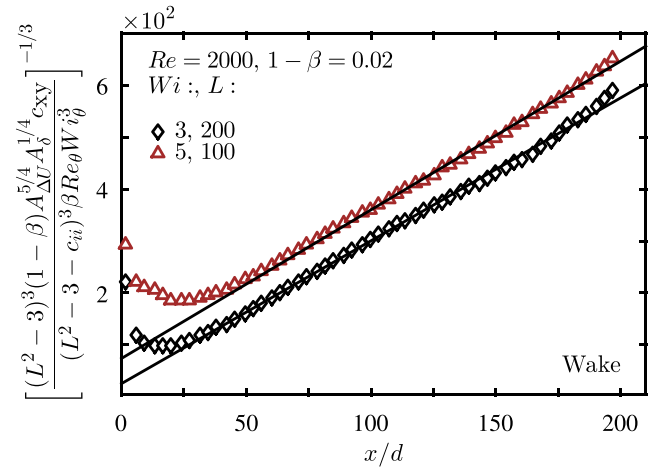


Fig. 10. Streamwise evolution of normalized $c_{xy}(x)$ compared to the theory for turbulent wakes at the highly-stretched nearly-isotropic regime. The solid curves are straight line fits to the DNS data.

5.2. Nearly-coiled nearly-isotropic regime

At the nearly-coiled nearly-isotropic regime the balance equation for $\overline{C_{xy}}$ is

$$\overline{C_{yy}} \frac{\partial \bar{u}}{\partial y} = \frac{\sigma_{xy}^{[p]}}{\rho \nu^{[p]}}, \quad (33)$$

and Eq. (21) gives the balance for the normal components and trace. This has been verified in Section 3 (cf. Fig. 4c) and is also demonstrated in more detail in Appendix B. The scaling of the turbulent polymer stretching tensor is

$$\frac{2\zeta c'_{ij} \partial u'_i / \partial x_j}{\beta De Re_{\theta} A_{\delta^2}^{5/4} A_{\Delta U}^{1/4} \Delta U / \delta} = N_{ij} \left(\frac{y}{\delta} \right), \quad (34)$$

$$\frac{c'_{xk} \partial v'_k / \partial x_k + c'_{yk} \partial u'_k / \partial x_k}{c_{yy} A_{\delta^2} u^* / r^*} = N_{xy} \left(\frac{y}{\delta} \right), \quad (35)$$

where Eq. (34) is for the normal components and trace and was obtained from Eq. (18) with (19). The validity of these scaling relations of the nearly-coiled nearly-isotropic regime is verified at Fig. 11: when profiles at different x/d stations are normalized with the proposed scaling they all collapse onto single curves for each quantity.

The shear component of the turbulent polymer stretching tensor does not appear in the balance Eq. (33) for $\overline{C_{xy}}$ but the scaling (35) is important for the demonstration that Eq. (33) results from the general Eq. (8) in the limit condition of the nearly-coiled regime, as detailed in Appendix B. The spreading rate parameter of the wake, A_{δ^2} , has been introduced in Eq. (35) after an inspection of the resulting self-similarity equation of $\overline{C_{xy}}$. The $c_{yy}(x)$ component is used at Eq. (35) instead of $c_{xy}(x)$ because it was verified from the DNS data that this is the scaling that provides similarity of $N_{xy}(\xi)$ at the nearly-coiled regime. The relations given by Eqs. (22), (23) and (24) are also considered at the nearly-coiled regime, where the approximation $f(c_{nn} - 3) = 1$ is adopted to simplify the formulation, resulting in the following self-similarity equations at the limit case of the nearly-coiled nearly-isotropic regime

$$\frac{\beta De^2 Re_{\theta} A_{\delta^2}^{5/4} A_{\Delta U}^{1/4}}{\zeta c_{ij}} \left\{ N_{ij} \right\} = \left\{ \sigma_{ij} \right\}, \quad (36)$$

for the normal components and trace (no summation on ij) and

$$\frac{De}{c_{xy}} \left\{ \frac{d\psi}{d\xi} \right\} = \left\{ \sigma_{xy} \right\}, \quad (37)$$

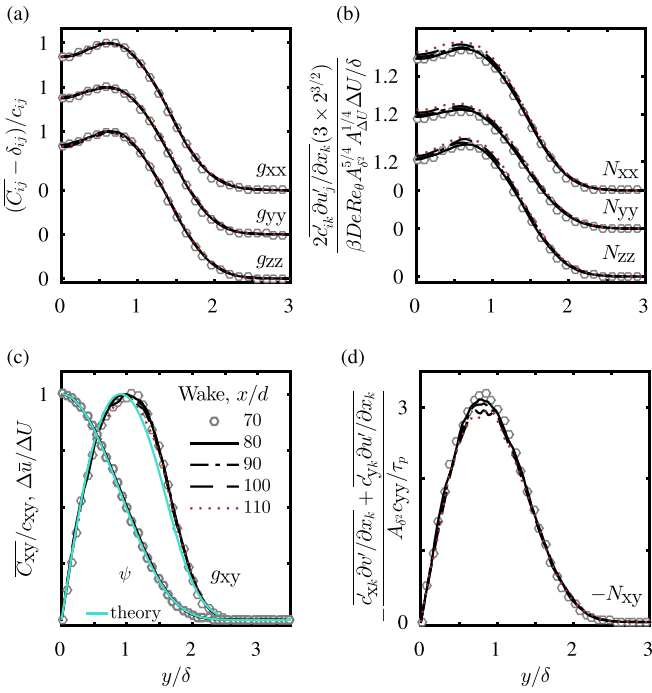


Fig. 11. Transverse profiles at different x/d stations, at the nearly-coiled nearly-isotropic regime, shown with similarity coordinates for a wake with $Wi = 0.15$, $Re = 4000$ and $1 - \beta = 0.20$: (a) normal components of g_{ij} , (b) normal components of N_{ij} , (c) shear component of g_{ij} and ψ , (d) shear component of N_{ij} .

for the shear component \overline{C}_{xy} . Using self-similarity arguments similar to those of Section 5.1 we obtain the scaling laws for $c_{ij}(x)$ at the nearly-coiled nearly-isotropic regime. For the normal components and trace, the result is

$$\left[\frac{c_{ij}(x)}{\beta Wi_\theta^2 Re_\theta A_{\Delta U}^{-3/4} A_{\delta^2}^{9/4}} \right]^{-1/2} = A_{c_{ij}} \left(\frac{x - x_0}{\theta} \right). \quad (38)$$

For the shear component we obtain

$$\left[\frac{c_{xy}(x)}{Wi_\theta (A_{\Delta U} A_{\delta^2})^{-1/2}} \right]^{-1} = A_{c_{xy}} \left(\frac{x - x_0}{\theta} \right), \quad (39)$$

where $A_{c_{ij}}$ are scaling law coefficients.

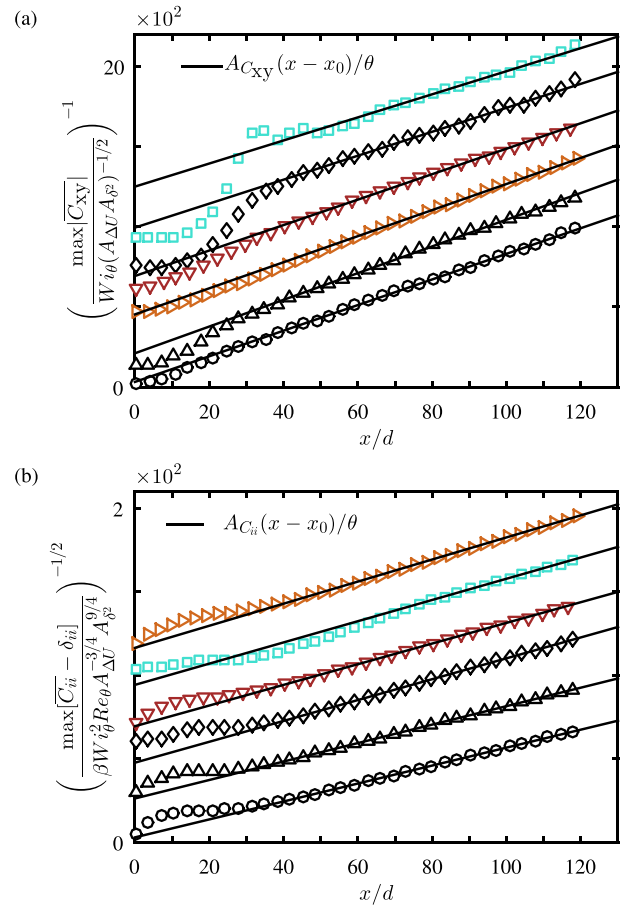
Fig. 12 compares the DNS results with the scaling laws of Eqs. (38) and (39). Good agreement is obtained between the theory and the data. The curves shown at Fig. 12 are approximately parallel at the far field and so $A_{c_{ij}}$ is approximately independent of Wi_θ , Re_θ and β , suggesting another interesting result: the shear component of the conformation tensor grows linearly with the inlet Wi_θ , while the extension of polymer chains grows with $\beta Wi_\theta^2 Re_\theta$. This can be seen by isolating $c_{ij}(x)$ in Eqs. (38) and (39). The result is compared against the DNS data at Fig. 13. Again, good agreement is obtained.

5.3. Nearly-coiled final region of decay

The balance equations for \overline{C}_{xx} and \overline{C}_{yy} at the nearly-coiled final region of decay are

$$2\overline{C}_{xx} \frac{\partial \bar{u}}{\partial x} = \frac{\overline{\sigma_{xx}}^{[p]}}{\rho \nu^{[p]}}, \quad 2\overline{C}_{yy} \frac{\partial \bar{v}}{\partial y} = \frac{\overline{\sigma_{yy}}^{[p]}}{\rho \nu^{[p]}}, \quad (40a,b)$$

respectively, while the equation for \overline{C}_{xy} is given by Eq. (33), and for the \overline{C}_{zz} component and trace \overline{C}_{ii} by Eq. (21). This has been shown in Section 3 (cf. Fig. 4h) and is also demonstrated in more detail in Appendix B.



$Re = 4000$, $1 - \beta = 0.20$, $1 - \beta = 0.02$
 $1 - \beta = 0.20, Wi :$ $Wi = 0.15, Re :$ $Re = 4000, Wi :$
 $\circ 0.05 \quad \triangle 0.15 \quad \diamond 0.3$ $\triangleright 1500 \quad \triangleright 3000$ $\square 0.3$

Fig. 12. Streamwise evolution of normalized $c_{ij}(x)$ compared to the theory for turbulent wakes at the nearly-coiled nearly-isotropic regime: (a) shear component, (b) trace. For clarity, different vertical shifts have been applied to each curve. For $c_{ii}(x)$, from top to bottom curves the shifts are equal to 112 (light brown circles), 97 (cyan circles), 65 (brown triangles), 55 (black diamonds), 25 (black triangles), and 0 (black circles). For $c_{xy}(x)$, from top to bottom curves the shifts are equal to 920 (cyan circles), 740 (black diamonds), 600 (brown triangles), 440 (light brown circles), 120 (black triangles), and 0 (black circles).

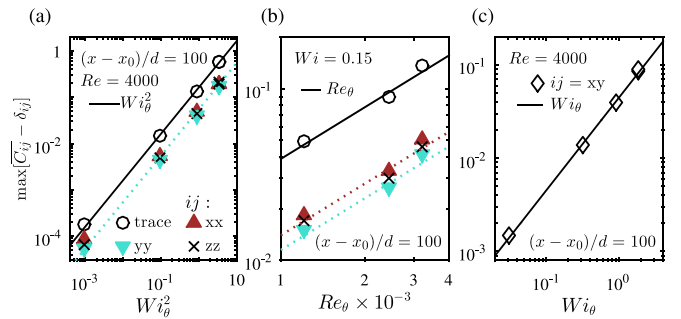


Fig. 13. DNS wake data are compared to analytical predictions. The figures show the influence of inlet and rheological parameters on the far field conformation tensor at the nearly-coiled nearly-isotropic regime: (a) and (b) normal components and trace, (c) shear component.

Adopting the same scaling relations of Section 5.2 and considering the limit condition detailed at the beginning of Section 5 leads to

$$\pm \frac{De}{c_{xx,yy} \delta} \frac{d\delta^2}{dx} \left\{ \psi + \xi \frac{d\psi}{d\xi} \right\} = \left\{ \sigma_{xx,yy} \right\} \quad (41)$$

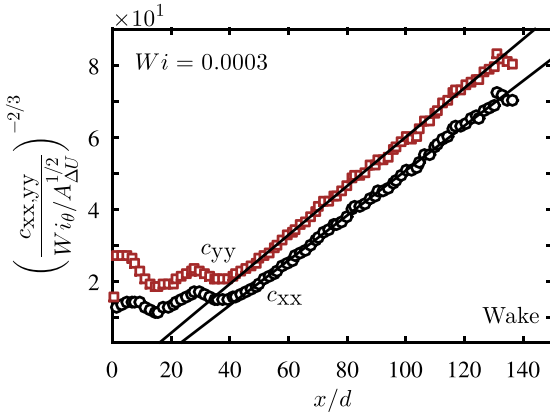


Fig. 14. Streamwise evolution of normalized $c_{xx}(x)$ and $c_{yy}(x)$ from DNS (symbols, $Re = 1500$, $Wi = 0.0003$, $L = 100$, and $1 - \beta = 0.20$) compared to the theory (straight lines) for turbulent wakes at the nearly-coiled final region of decay. The $c_{yy}(x)$ curve (brown squares) has been shifted upward by 5 units, for clarity.

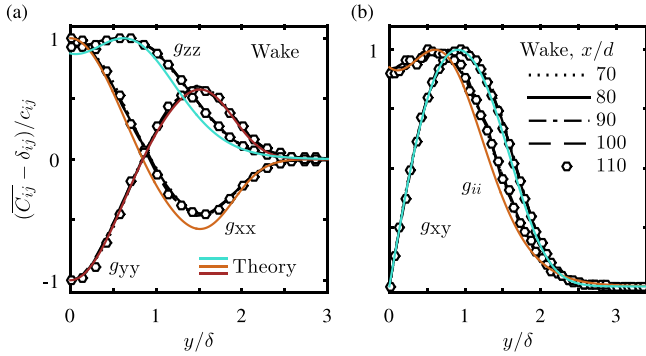


Fig. 15. Transverse profiles of normalized conformation tensor components and trace from wake DNS ($Re = 1500$, $Wi = 0.0003$, $L = 100$, and $1 - \beta = 0.20$) at different x/d stations at the final region of decay compared with analytical predictions: (a) normal components of g_{ij} , (b) shear component and trace of g_{ij} .

where the subscript xx,yy refers to the result for the xx or yy normal components, respectively, and \pm is a plus sign for xx and a minus sign for yy . Using similar arguments as before will lead to

$$\left[\frac{c_{xx,yy}(x)}{Wi^2/A_\delta^{1/2}} \right]^{-2/3} = \tilde{A}_{c_{xx,yy}} \left(\frac{x - x_0}{d} \right), \quad (42)$$

where $\tilde{A}_{c_{xx,yy}}$ are scaling law coefficients. These laws for $c_{xx,yy}(x)$ at the final region of decay are compared against the DNS data in Fig. 14, showing good agreement between the theory and the data. The other components of $c_{ij}(x)$ follow the scaling laws derived and validated in Section 5.2 and thus are not shown in Fig. 14.

The scatter observed in the curves of Fig. 14 is due to an insufficient level of statistical convergence, which is difficult to obtain for that case since the Runge–Kutta time step of the simulation had to be decreased significantly in order to maintain stable computations. The numerical instability at very low τ_p results from the fact that, in this case, the polymer stress in Eq. (2) is a very small number resulting from the division of two very small numbers (τ_p and $C - I$), a situation that is prone to numerical problems. Presumably this could be alleviated using the fact that $v^{[p]}$ is proportional to τ_p when $\tau_p \rightarrow 0$ [32], but this has not been tested.

The transverse profiles of $\overline{C_{ij}} - \delta_{ij}$ at the final region of decay are shown in Fig. 15, where some analytical solutions to be discussed in Section 7 are also shown for comparison.

6. Similarity laws of the conformation tensor: planar jet

The theory for the planar jet follows similar lines as those described above for the planar wake. Thus, we only show some aspects of the analysis that are different for jets and wakes and present the final results and comparisons with the DNS data. The balance equations (without normalizations) for $\overline{C_{ij}}$ at the different polymer deformation regimes are the same for jets and wakes. The turbulent velocity scale of the viscoelastic planar jet is different and equal to [9]

$$u' \sim U_c \frac{d\delta}{dx}, \quad (43)$$

which results in different scaling relations for the normal components and trace of the turbulent polymer stretching tensor. Furthermore, the momentum integral constraint of viscoelastic turbulent planar jets is given by $d[U_c(x)^2 \delta(x)]/dx = 0$ [9]. The local Reynolds number $Re_\delta(x) = U_c(x)\delta(x)/\nu^{[s]}$ is high and the non-dimensional spreading rate coefficient $A_\delta = d\delta(x)/dx$ is small. The self-similarity relation of the mean velocity is

$$\frac{\bar{u}}{U_c} = \psi \left(\frac{y}{\delta} \right). \quad (44)$$

The results for the highly-stretched nearly-isotropic regime are shown at Section 6.1, for the nearly-coiled nearly-isotropic regime at Section 6.2 and for the nearly-coiled final region of decay in Section 6.3. Some details of the derivation are presented in Appendix B.

6.1. Highly-stretched nearly-isotropic regime

The scaling of the normal components and trace of the turbulent polymer stretching tensor that is obtained from Eq. (13) with Eq. (43) is

$$\frac{2\zeta f(c_{nn} + 3)\overline{c'_{ik} \partial u'_j / \partial x_k}}{[\beta/(1 - \beta)]DeRe_\delta A_\delta^{3/2} U_c / \delta} = N_{ij} \left(\frac{y}{\delta} \right), \quad (45)$$

where $\zeta = 1$ for the trace and $\zeta = 3$ for each normal component. For the shear component, the scaling is given by

$$\frac{c'_{xk} \partial v' / \partial x_k + c'_{yk} \partial u' / \partial x_k}{A_\delta^{-1} f(c_{nn} + 3)c_{xy} u^* / r^*} = N_{xy} \left(\frac{y}{\delta} \right), \quad (46)$$

which is very similar to the scaling used for wakes, given by Eq. (26), but the inverse of the constant spreading rate coefficient A_δ^{-1} has been introduced to make N_{xy} order unity.

The resulting self-similarity equations are

$$\frac{\beta De^2 Re_\delta}{(1 - \beta)\zeta f(c_{nn} + 3)c_{ij}} \left(\frac{d\delta}{dx} \right)^{3/2} \left\{ N_{ij} \right\} = \left\{ \sigma_{ij} \right\}, \quad (47)$$

for the normal components and trace (no summation on ij) and for the shear component we obtain

$$-\frac{A_\delta De c_{yy}}{f(c_{nn} + 3)c_{xy}} \left\{ g_{yy} \frac{d\psi}{d\xi} \right\} = \left\{ N_{xy} \right\} - A_\delta \left\{ \sigma_{xy} \right\}. \quad (48)$$

The resulting scaling laws are

$$\left\{ \frac{(L^2 - 3)^2 (1 - \beta) A_\delta^{3/2} c_{ij}(x)}{[L^2 - 3 - c_{nn}(x)]^2 \beta Wi^2 Re A_\delta^{1/2}} \right\}^{-2/5} = \overline{A}_{c_{ij}} \left(\frac{x - x_0}{h} \right), \quad (49)$$

for the normal components and trace and

$$\left\{ \frac{(L^2 - 3)^3 (1 - \beta) A_\delta^2 A_\delta^{-1/2} c_{xy}(x)}{[L^2 - 3 - c_{nn}(x)]^3 \beta Wi^3 Re} \right\}^{-1/4} = \overline{A}_{c_{xy}} \left(\frac{x - x_0}{h} \right), \quad (50)$$

for the shear component. For thin shear-layers at high Re the spreading rate parameter $A_\delta = d\delta/dx$ is small and the shear relaxation term of Eq. (48) can be neglected as a first order approximation. Nevertheless, since A_δ is constant at the far-field [9] neglecting or retaining this term leads to the exactly same scaling law for $c_{xy}(x)$.

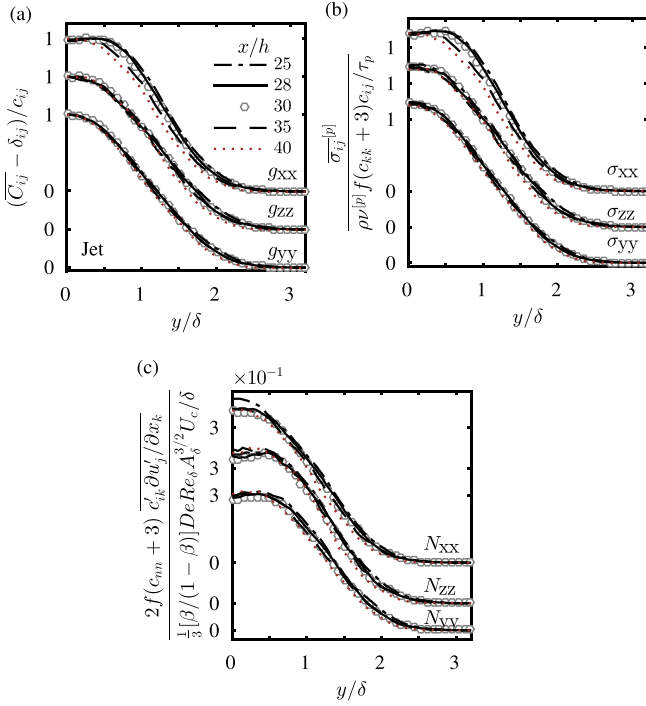


Fig. 16. Transverse profiles at different x/h stations normalized according to the proposed theory at the highly-stretched nearly-isotropic regime: normal components of (a) g_{ij} , (b) σ_{ij} and (c) N_{ij} , for the jet with $Wi = 5$, $Re = 2500$, $1 - \beta = 0.02$ and $L = 200$.

Transverse profiles at different x stations, normalized according to the theory of the turbulent planar jet, are displayed at Figs. 16 and 17, for normal and shear components, respectively. When the proposed normalization is adopted, the profiles collapse onto single curves for each quantity. Because the similarity region of the shear component starts later than those of the normal components, a DNS with a very large computational domain ($L_x/h = 97.8$) was performed to verify the scaling law for $c_{xy}(x)$. However, we were unable to obtain a perfect level of statistical convergence for this case, due the very high computational cost of this simulation. The transverse profiles of g_{xy} and σ_{xy} are not shown for this reason, but as mentioned in the paragraph above, to a leading order approximation self-similarity of these profiles is not required for the derivation of the $c_{xy}(x)$ scaling law for the jet flow configuration at the highly-stretched nearly-isotropic regime.

The validity of the scaling laws given by Eqs. (49) and (50) is confirmed in Figs. 18 and 19 for the trace and shear component, respectively, exhibiting good agreement between the theory and the DNS. A similar level of agreement has been obtained for the normal components individually (not shown).

6.2. Nearly-coiled nearly-isotropic regime

At the nearly-coiled nearly-isotropic regime the resulting scaling of the $N_{ij}(\xi)$ normal components and trace is

$$\frac{2\zeta c'_{ik} \partial u'_j / \partial x_k}{\beta De Re_\delta A_\delta^{3/2} U_c / \delta} = N_{ij}(y/\delta), \quad (51)$$

which is obtained from Eq. (18) with Eq. (43), and for the shear component the scaling is given by Eq. (35) with A_δ instead of $A_{\delta 2}$. The self-similarity equations are

$$\frac{\beta De^2 Re_\delta A_\delta^{3/2}}{\zeta c_{ij}} \left\{ N_{ij} \right\} = \left\{ \sigma_{ij} \right\}, \quad (52)$$

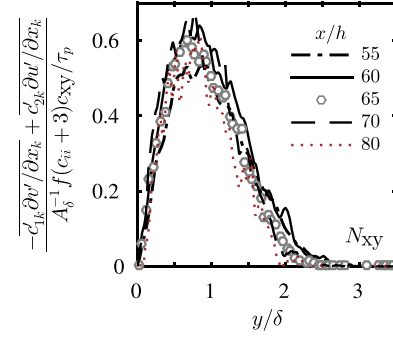


Fig. 17. Transverse profiles of the shear component of the turbulent polymer stretching tensor (N_{xy}), at different x/h stations at the highly-stretched nearly-isotropic regime shown with similarity coordinates for the jet with $Wi = 5$, $Re = 2500$, $1 - \beta = 0.02$ and $L = 200$.

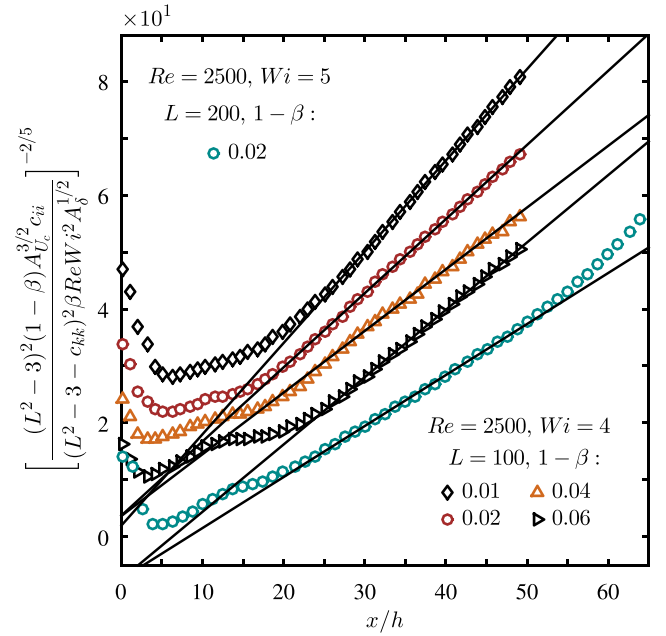


Fig. 18. Streamwise evolution of the normalized trace $c_{ii}(x)$ compared to the theory for turbulent jets at the highly-stretched nearly-isotropic regime. Solid curves are straight line fits to the DNS data. Vertical shifts are applied for clarity. From top to bottom curves the shifts are equal to 12 (black diamonds), 8 (brown triangles), 0 (black laying triangles), and -7 (dark cyan circles).

for the normal components and trace of $\overline{C_{ij}}$ (no summation on ij) and (37) for the shear component. The resulting scaling laws are given by

$$\left[\frac{c_{ij}(x)}{\beta Wi^2 Re A_\delta^{1/2} / A_c^{3/2}} \right]^{-2/5} = A_{c_{ij}} \left(\frac{x - x_0}{h} \right), \quad (53)$$

for the normal components and trace and by

$$\left[\frac{c_{xy}(x)}{Wi A_c^{-1/2} A_\delta^{-1}} \right]^{-2/3} = A_{c_{xy}} \left(\frac{x - x_0}{h} \right). \quad (54)$$

for the shear component.

Transverse profiles at different x stations collapse into a single curve when normalized according to the proposed theory (Fig. 20). As shown in Fig. 21, good agreement is obtained between the scaling laws and the DNS data at the far field. As in the wake flow configuration, the lines displayed at Fig. 21 for jets are approximately parallel and the $A_{c_{ij}}$ coefficients are independent to the inlet Re , Wi and β parameters, suggesting a $\beta Wi^2 Re$ dependence of $\overline{C_{ij}}$ at the far field, for the normal

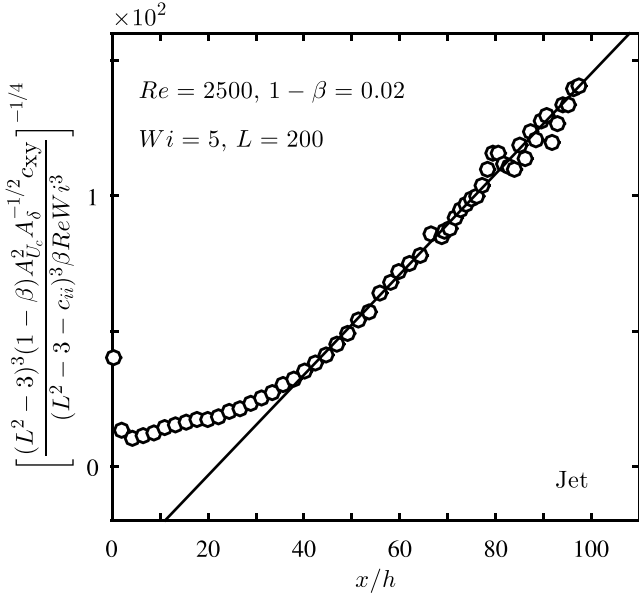


Fig. 19. Streamwise evolution of normalized $c_{xy}(x)$ compared to the theory for turbulent jets at the highly-stretched nearly-isotropic regime. The solid curve is a straight line fit to the DNS data.

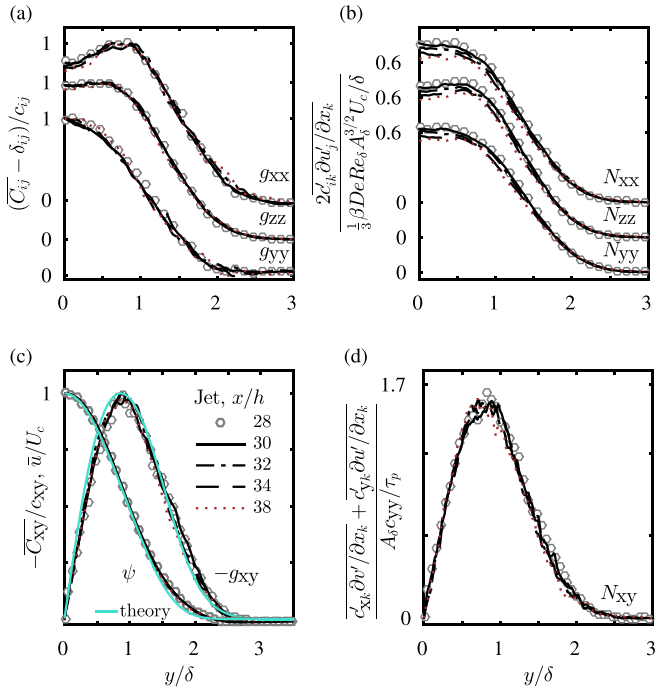


Fig. 20. Transverse profiles at the nearly-coiled nearly-isotropic regime shown with similarity coordinates for a jet with $Wi = 0.15$, $Re = 3500$ and $1 - \beta = 0.20$: (a) normal components of g_{ij} , (b) normal components of N_{ij} , (c) shear component of g_{ij} and ψ , (d) shear component of N_{ij} .

components and trace, and a linear Wi dependence for the \overline{C}_{xy} components. This can be seen by isolating $c_{ij}(x)$ in Eqs. (53) and (54), and the result is confirmed at Fig. 22.

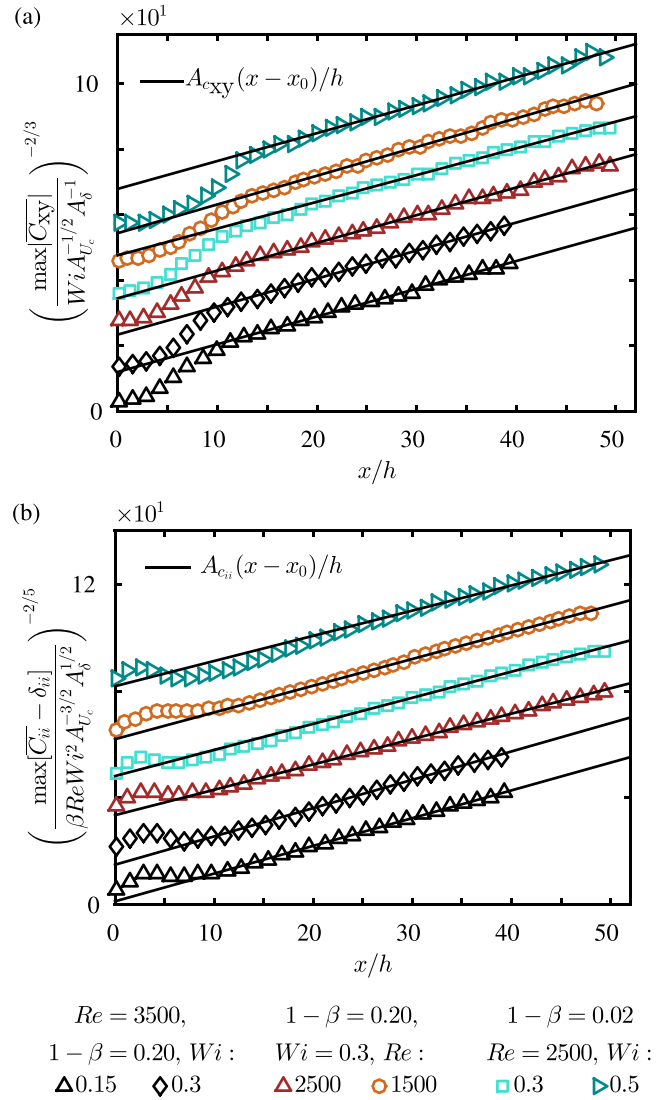


Fig. 21. Streamwise evolution of normalized $c_{ij}(x)$ compared to the theory for turbulent jets at the nearly-coiled nearly-isotropic regime: (a) shear component, (b) trace. For clarity, different vertical shifts have been applied to each curve. For $c_{ii}(x)$, from top to bottom curves the shifts are equal to 80 (dark cyan laying triangles), 62 (light brown circles), 44 (cyan squares), 32 (brown triangles), 16 (black diamonds), and 0 (black triangles). For $c_{xy}(x)$, from top to bottom curves the shifts are equal to 55 (dark cyan laying triangles), 43 (light brown circles), 33 (cyan squares), 25 (brown triangles), 11 (black diamonds), and 0 (black triangles).

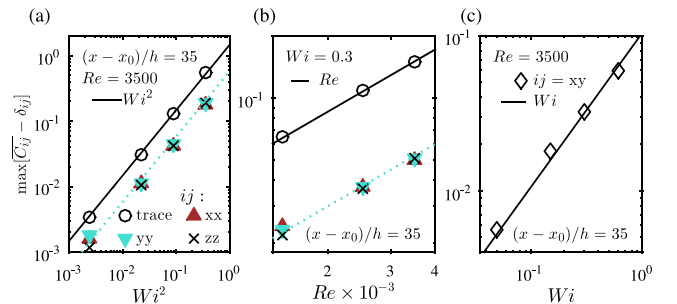


Fig. 22. DNS jet data are compared to analytical predictions. The figures show the influence of inlet and rheological parameters on the far-field conformation tensor at the nearly-coiled nearly-isotropic regime: (a) and (b) normal components and trace, (c) shear component.

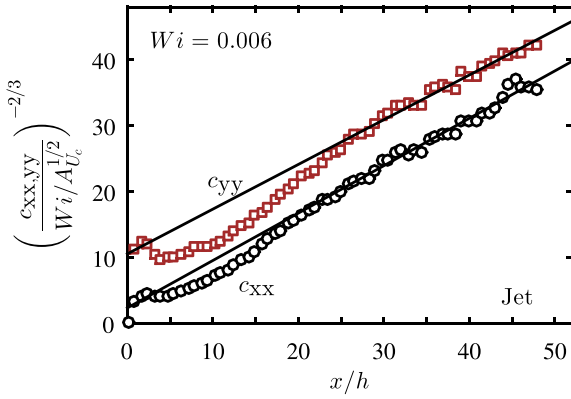


Fig. 23. Streamwise evolution of normalized $c_{xx}(x)$ and $c_{yy}(x)$ from DNS (symbols, $Re = 2000$, $Wi = 0.006$, $L = 100$, and $1 - \beta = 0.20$) compared to the theory (straight lines) for turbulent jet at the nearly-coiled final region of decay. The $c_{yy}(x)$ curve (brown squares) has been shifted upward by 5 units, for clarity.

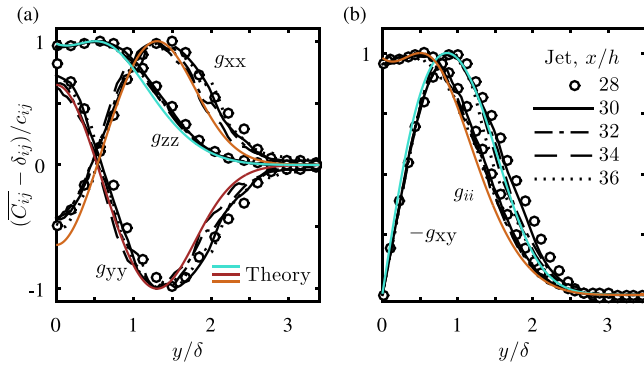


Fig. 24. Transverse profiles of normalized conformation tensor components and trace from jet DNS ($Re = 2000$, $Wi = 0.006$, $L = 100$, and $1 - \beta = 0.20$) at different x/h stations at the final region of decay compared with analytical predictions: (a) normal components of g_{ij} , (b) shear component and trace of g_{ij} .

6.3. Nearly-coiled final region of decay

The self-similarity equation for $\overline{C_{xx}}$ and $\overline{C_{yy}}$ at the final region of decay is

$$\mp \frac{De(x)}{c_{xx,yy}(x)} \frac{d\delta}{dx} \left\{ \psi + 2\xi \frac{d\psi}{d\xi} \right\} = \left\{ \sigma_{xx,yy} \right\}, \quad (55)$$

and the resulting scaling laws are given by

$$\left[\frac{c_{xx,yy}(x)}{Wi/A Uc^2} \right]^{-2/3} = \tilde{A}_{c_{xx,yy}} \left(\frac{x - x_0}{h} \right). \quad (56)$$

The scaling laws are compared to the DNS data in Fig. 23, showing good agreement at the far field. The data scatter observed in Fig. 23 is due to the very small Runge–Kutta time step of this simulation, which makes it difficult to obtain a perfect level of statistical convergence for that case (cf. the detailed explanation at Section 5.3).

Transverse profiles are displayed at Fig. 24, where some analytical results to be presented in Section 7 are also shown for comparison—again, good agreement is obtained between the theory and the DNS data.

7. Asymptotic solutions for the transverse profiles at the final region of decay

The scaling laws presented at Sections 5 and 6 have been derived from scaling analyses and asymptotic considerations that make no use

of any turbulence model for unclosed terms of the governing equations. These laws provide a detailed description for the downstream evolution of the conformation and polymer stretching tensors in terms of inlet and rheological parameters Re , Wi , β , L , and the distance x from the jet orifice or wake object, and the self-similarity relations for the transverse y profiles. However, they do not describe the variation of these tensors on the y direction *i.e.* the geometrical form of the transverse profiles. In the present section we obtain the solutions for the self-similar transverse profiles of the conformation tensor components $g_{ij}(\xi)$ at the final region of decay, providing the complete solution for the mean field problem at $x \rightarrow \infty$, which is a limit case that has always received considerable attention for both laminar and turbulent shear flows. In fact, the solutions obtained here for $g_{xx}(\xi)$, $g_{yy}(\xi)$ and $g_{zz}(\xi)$ are valid only at the final region of decay, but the solutions for $g_{xy}(\xi)$ and the trace $g_{ii}(\xi)$ are also valid at the nearly-coiled nearly-isotropic sub-regime (see Appendix C for a discussion on the domain of validity of the results).

From the self-similarity balance equations given by Eqs. (37) and (41), for wakes, and (37) and (55), for jets, it is clear that $\sigma_{xx}(\xi)$ and $\sigma_{yy}(\xi)$ at the final region of decay and $\sigma_{xy}(\xi)$ at the nearly-coiled regime can be obtained directly from the normalized mean velocity profile $\psi(\xi)$, which is known to be the same as for a Newtonian fluid ([9,10] and references therein). The expression for $\psi(\xi)$ is obtained from eddy viscosity and mixing length arguments and a correction that accounts for the intermittent character of the position of the irrotational boundary. The adopted expression for the turbulent shear stress is

$$-\overline{u'v'} = \nu_t \partial \bar{u} / \partial y, \quad (57)$$

where $\nu_t(x) = \tilde{\nu}_t u'(x) \delta(x)$ is the eddy viscosity and $\tilde{\nu}_t$ is a constant model parameter. The two-state intermittency model, proposed originally for boundary layers [33–35] and that has some similarities with models for turbulent premixed flames [36], is used here for the irrotational boundary intermittency correction.

The details of the derivation of the $g_{xx}(\xi)$, $g_{yy}(\xi)$ and $g_{xy}(\xi)$ closed form analytical solutions, using the procedure described above, are given at Appendix D. These analytical solutions are compared to the DNS data in Figs. 11 and 15, for wakes, and in Figs. 20 and 24, for jets, showing good agreement.

To calculate the profiles of $\overline{C_{ii}}$ and $\overline{C_{zz}}$ at $x \rightarrow \infty$ an expression for the turbulent stretching term $2c'_{ik} \partial u'_i / \partial x_k$ is needed. This will be obtained from the solution of the transport equation of κ , which for a steady mean flow is given by

$$\begin{aligned} \bar{\mathbf{u}} \cdot \nabla \kappa &= -\nabla \cdot \overline{p' \mathbf{u}'} / \rho - \nabla \cdot \overline{\mathbf{u}' \mathbf{u}' \cdot \mathbf{u}'} / 2 + \nu^{[s]} \nabla^2 \kappa \\ &\quad - \overline{\mathbf{u}' \mathbf{u}'} : \nabla \bar{\mathbf{u}} - \nu^{[s]} \nabla \mathbf{u}' : \nabla \mathbf{u}' \\ &\quad + \nabla \cdot \sigma'^{[p]} \cdot \mathbf{u}' / \rho - \varepsilon^{[p]}. \end{aligned} \quad (58)$$

Neglecting the viscoelastic advection term $\nabla \cdot \sigma'^{[p]} \cdot \mathbf{u}' / \rho$, that is much smaller than the dominant terms [9,10] and considering the closure assumptions of Prandtl (1945) [37] for the unclosed Newtonian turbulent diffusion and turbulent production terms of the equation (see also Wilcox 1998 [38] chapter 4) *i.e.*

$$-\nabla \cdot \overline{p' \mathbf{u}'} / \rho - \nabla \cdot \overline{\mathbf{u}' \mathbf{u}' \cdot \mathbf{u}'} / 2 = (\nu_t / A_\sigma) \partial^2 \kappa / \partial y^2, \quad (59)$$

$$-\overline{\mathbf{u}' \mathbf{u}'} : \nabla \bar{\mathbf{u}} = \nu_t (\partial \bar{u} / \partial y)^2, \quad (60)$$

where A_σ is a constant model parameter, we arrive at a closed equation for κ when the following assumption is invoked:

$$\varepsilon^{[p]} + \varepsilon^{[s]} = A_\varepsilon \frac{\kappa^{3/2}}{\delta}, \quad (61)$$

which is analogous to the extended dissipation law of Eq. (9), but with an equality sign and a dimensionless proportionality coefficient A_ε .

Combining Eq. (61) with the scaling law for the solvent dissipation reduction parameter SDR of Eq. (16), the balance equation for the trace $\overline{C_{ii}}$ (Eq. (21)), together with the Oldroyd-B approximation to

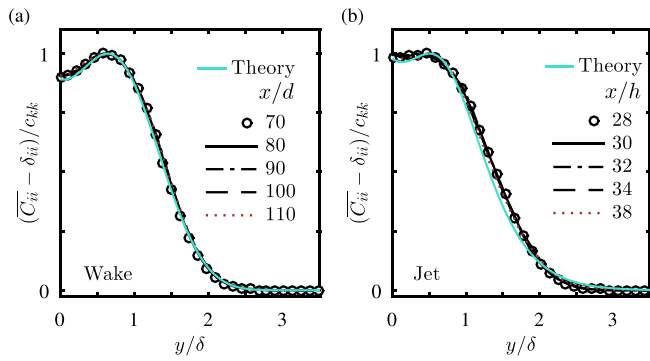


Fig. 25. Transverse profiles of normalized polymer chain extension at different x stations at the nearly-coiled nearly-isotropic regime for (a) wake with $Wi = 0.15$, $Re = 4000$ and $1 - \beta = 0.20$ and (b) jet with $Wi = 0.15$, $Re = 3500$ and $1 - \beta = 0.20$.

relate $\overline{C_{ii}}$ with $\overline{\sigma_{ii}^{[p]}}$, and $\varepsilon^{[p]}$ with $2c'_{ik}\partial u'_i/\partial x_k$ (cf. end of Section 4.2), we obtain

$$\overline{C_{ii}} - \delta_{ii} = \frac{\tau_p^2}{\sqrt{[p]}}(1 - \beta)A_{SDR}A_\varepsilon \frac{\kappa^{3/2}}{\delta}, \quad (62)$$

so that the solution for $\overline{C_{ii}} - \delta_{ii}$ can be obtained from the solution for κ . Considering the self-similar turbulent kinetic energy profile

$$K(y/\delta(x)) = \kappa(x, y)/(u'(x)^2), \quad (63)$$

the balance equation for κ , written with similarity variables, is obtained and solved for jets and wakes after the introduction of the corresponding turbulent velocity scales $u'(x)$. The resulting profiles of κ are also corrected to account for the intermittent character of the turbulent interface, similarly to the correction made for the mean velocity—Krug et al. (2017) [34] have shown that the two state intermittency model is also valid for the turbulent velocity fluctuations.

More details on the derivation of the analytical solution for $g_{ii}(\xi)$ are given at Appendix D, where the final form of the obtained $g_{ij}(\xi)$ solutions are also shown. For wakes, a closed-form analytical solution is derived for $g_{ii}(\xi)$ and $g_{zz}(\xi)$. For jets, a numerical solution for $g_{ii}(\xi)$ and $g_{zz}(\xi)$ is obtained, since we were not able to solve the ordinary differential equation (ODE) analytically for jets (see Appendix D).

The analytical and numerical solutions are compared to the DNS data in Figs. 15 and 25a, for wakes, and in 24 and 25b, for jets. As before, good agreement is obtained between the theory and the data.

8. Summary of main results and conclusion

A new theory has been formulated for the description of the conformation state of the polymer chains in free turbulent shear flows with viscoelastic fluids. The theory is based on a similarity analysis of the equations governing the evolution of each component and trace of the mean conformation tensor. The crucial assumption is the scaling of the turbulent polymer stretching tensor, whose trace is responsible for the energy flux between the turbulent kinetic energy of the flow and the mean elastic energy of the polymer chains. Two different scalings have been developed for the limits of low and high elasticity corresponding to the nearly-coiled and highly-stretched regimes of polymer deformation, respectively. These scalings are associated with the existence of minimum and maximum solvent dissipation reduction (*SDR*) asymptotes at these two limit cases. The maximum *SDR* asymptote is approximately invariant to rheological and flow parameters, similarly to the maximum drag reduction asymptote of turbulent pipe and channel flows, while the minimum *SDR* asymptote is proportional to the polymer concentration.

For each polymer deformation regime (nearly-coiled and highly-stretched) there are two sub-regimes, giving a total of four different sub-regimes of polymer deformation (see Fig. 1). At the highly-stretched anisotropic regime the scaling laws obtained by Guimarães (2020,2022) [9,10] apply. The present work focused on the three subsequent sub-regimes and a summary of all scaling laws is presented at the simplified diagram of Fig. 26, for turbulent planar jets and wakes.¹ The domains of validity of each scaling laws are delimited by the characteristic distances $\ell_{c_{ij}}$, also depicted in Fig. 26 and discussed at Appendix C. Since the flow strain rates responsible for the deformation of the polymer chains decay with x , it follows that different polymer deformation sub-regimes can exist sequentially in the same flow domain, but one may also have a single sub-regime. As shown at Appendix C, this will depend on how high the values of the inlet Wi and Re are and also on how large is the domain length L_x . Fig. 27 shows a case with a sufficiently large L_x so that two different sub-regimes can be observed in the flow. With a longer domain, the remaining two additional sub-regimes would be seen, but the simulation would be very costly.

All theoretical predictions have been validated through comparisons with results from new DNS of spatially evolving turbulent planar jets and wakes that make use of highly accurate numerical schemes and the FENE-P rheological model. Detailed theoretical studies of viscoelastic turbulent flows in general are hard to find, and often invoke exotic assumptions that are difficult to verify using results from DNS or experiments. In contrast, the present work is possibly the first where analytical predictions are obtained directly from the equations of the conformation tensor and where all hypothesis can be easily verified. We expect some of these ideas to be useful in the description of other spatially evolving canonical turbulent flows such as isotropic turbulence decaying behind a grid of bars, mixing-layers and the outer region of a flat plate boundary layer.

Declaration of competing interest

The authors declare that they have no known competing financial interests or personal relationships that could have appeared to influence the work reported in this paper.

Data availability

Data can be made available on reasonable request.

Acknowledgements

M.C.G acknowledges Fundação para a Ciência e Tecnologia (FCT) through contract UI/BD/151060/2021. C.B.S. acknowledges Fundação para a Ciência e Tecnologia (FCT) through IDMEC, under LAETA, project UIDB/50022/2020, and funding by FCT through project PCIF/MPG/0147/2019. F.T.P. is thankful for funding by FCT and Centro de Estudos de Fenómenos de Transporte through projects UIDB/00532/2020 and UIDP/00532/2020, and for funding by FCT and ALiCE through project LA/P/0045/2020.

¹ The scaling law of Guimarães et al. (2022) [10] for wakes appears here in a slightly modified format that contains the limit $\max|\overline{C_{ii}} - 3| \rightarrow L^2 - 3$ when $Re^2 Wi \rightarrow \infty$, which is obtained by the inclusion of a non-unitary Peterlin function, and the scaling law for jets was actually derived in the analogous way as done in Guimarães et al. (2022).

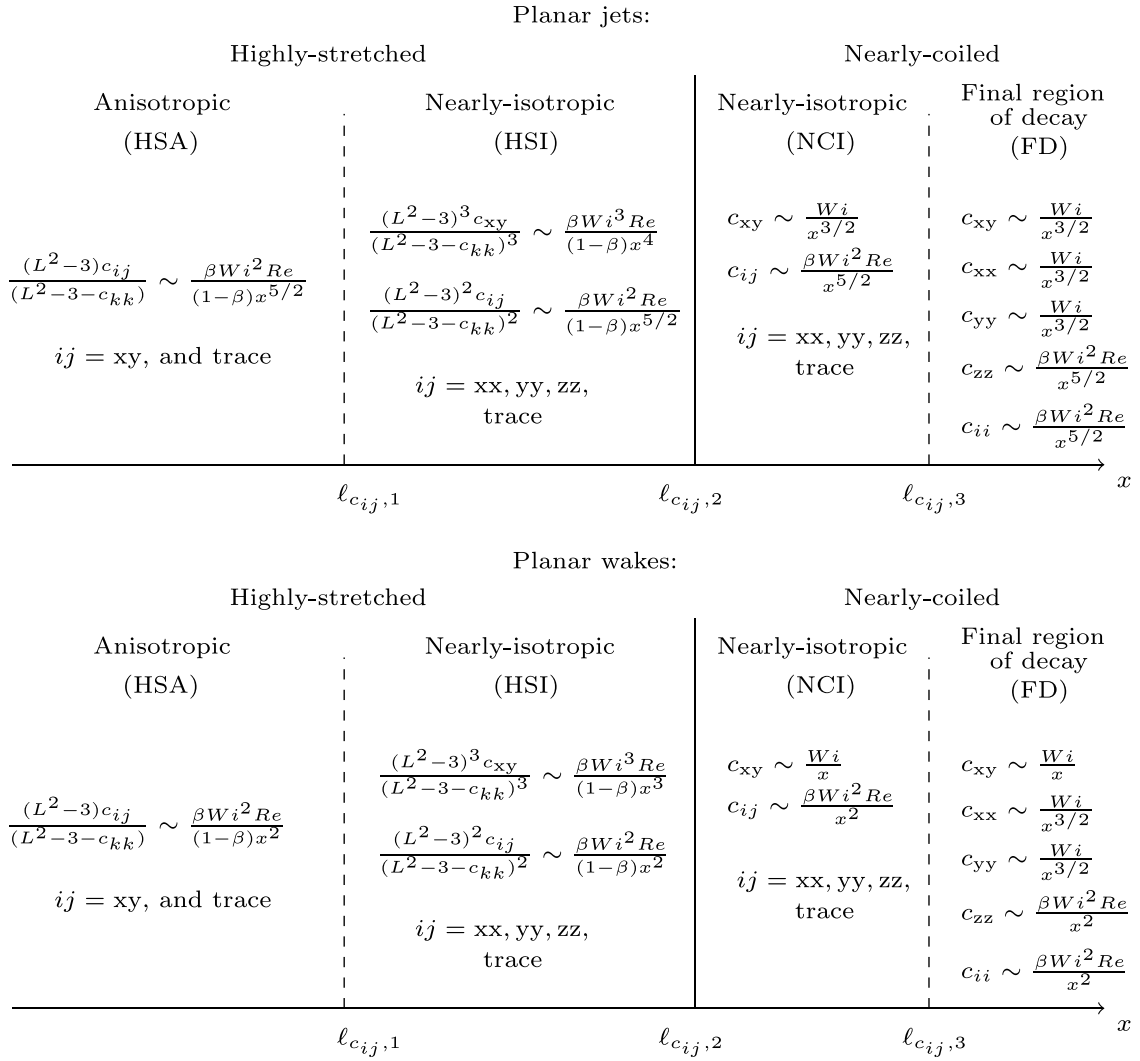


Fig. 26. Simplified diagram with a summary of the new scaling laws obtained for different polymer deformation regimes: (a) planar jets, (b) planar wakes. The theory describing the highly-stretched anisotropic sub-regime is presented at Guimarães (2020, 2022) [9,10]. The scale is arbitrary.

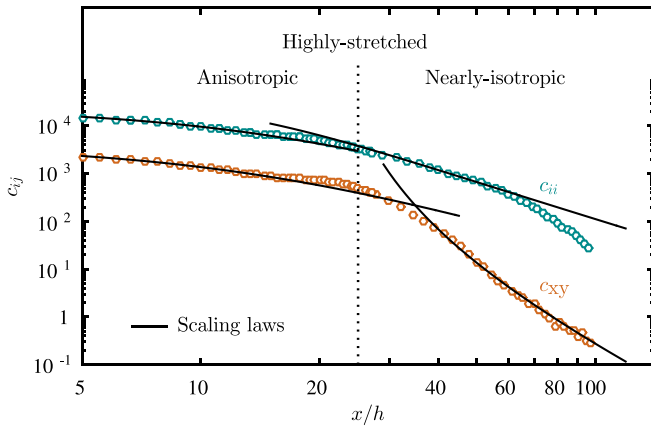


Fig. 27. Comparison between scaling laws for different polymer deformation regimes and the DNS data for a jet with $Re = 2500$, $Wi = 5$, $L = 200$ and $1-\beta = 0.02$. The domain length L_x is sufficiently large so that two different polymer deformation regimes can be observed in the same flow.

Appendix A. Budgets of the conformation tensor components: complementary data

This appendix shows the data that are complementary to the discussion of Section 3, concerning the budgets of the $\overline{C_{ij}}$ components. This is shown in Figs. A.28 and A.29, for jets and wakes, respectively.

Appendix B. Asymptotic limits of the conformation tensor equation

Here we show more details regarding the asymptotic evaluation of the balance equations for $\overline{C_{ij}}$, given by Eq. (8), that reduce to the simplified equations exposed at Sections 5 and 6 when the limit cases of the different polymer deformation regimes are considered. All terms of Eq. (8) are retained except the turbulent advection term. We start by normalizing each term of the equations according to the self-similarity transformations, and write the result so that terms inside curly brackets are $O(1)$ functions of $\xi = y/\delta(x)$ only. Thus, the order of magnitude of each term is given by the corresponding multiplying factors and the simplified equations of Sections 5 and 6 can be obtained as the distinguished limits of the general equation. The planar wake results are discussed in Appendix B.1 and the planar jet equations are shown in Appendix B.2. At each section, we start with the highly-stretched nearly-isotropic sub-regime, followed by the nearly-coiled sub-regimes.

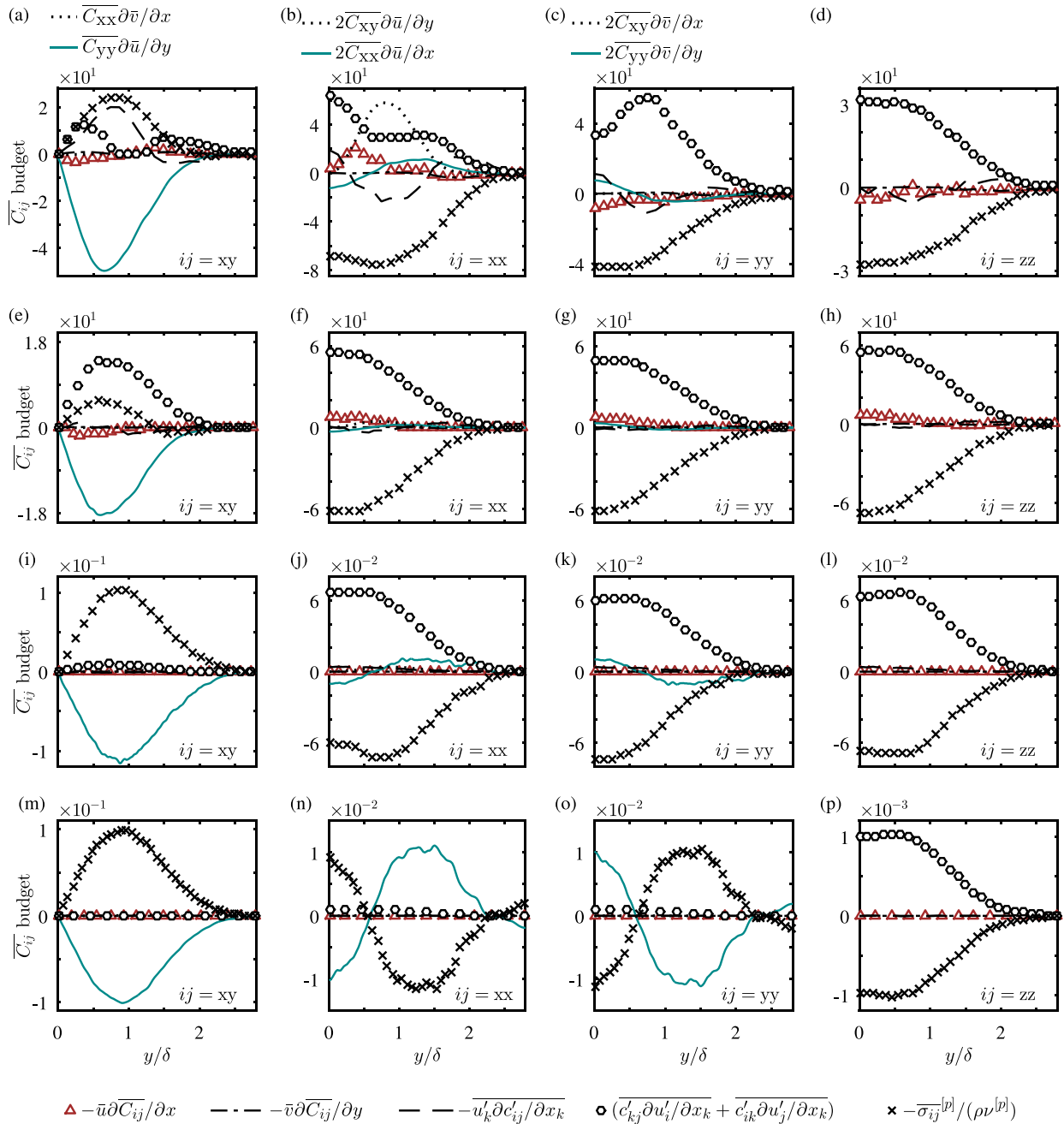


Fig. A.28. Budgets of $\overline{C_{ij}}$ for jets at different regimes of polymer chain deformation: (a-d) highly-stretched anisotropic, (e-h) highly-stretched nearly-isotropic, (i-l) nearly-coiled nearly-isotropic and (m-p) final region of decay. All quantities have been made non-dimensional using U_j and h . Flow conditions are: (a-d) $Re = 3500$, $Wi = 3$, $1 - \beta = 0.20$, $L = 100$, $x/h = 15$, (e-h) $Re = 2500$, $Wi = 4$, $1 - \beta = 0.02$, $L = 100$, $x/h = 35$, (i-l) $Re = 3500$, $Wi = 0.15$, $1 - \beta = 0.20$, $L = 100$, $x/h = 36$, (m-p) $Re = 1500$, $Wi = 0.006$, $1 - \beta = 0.20$, $L = 100$, $x/h = 40$.

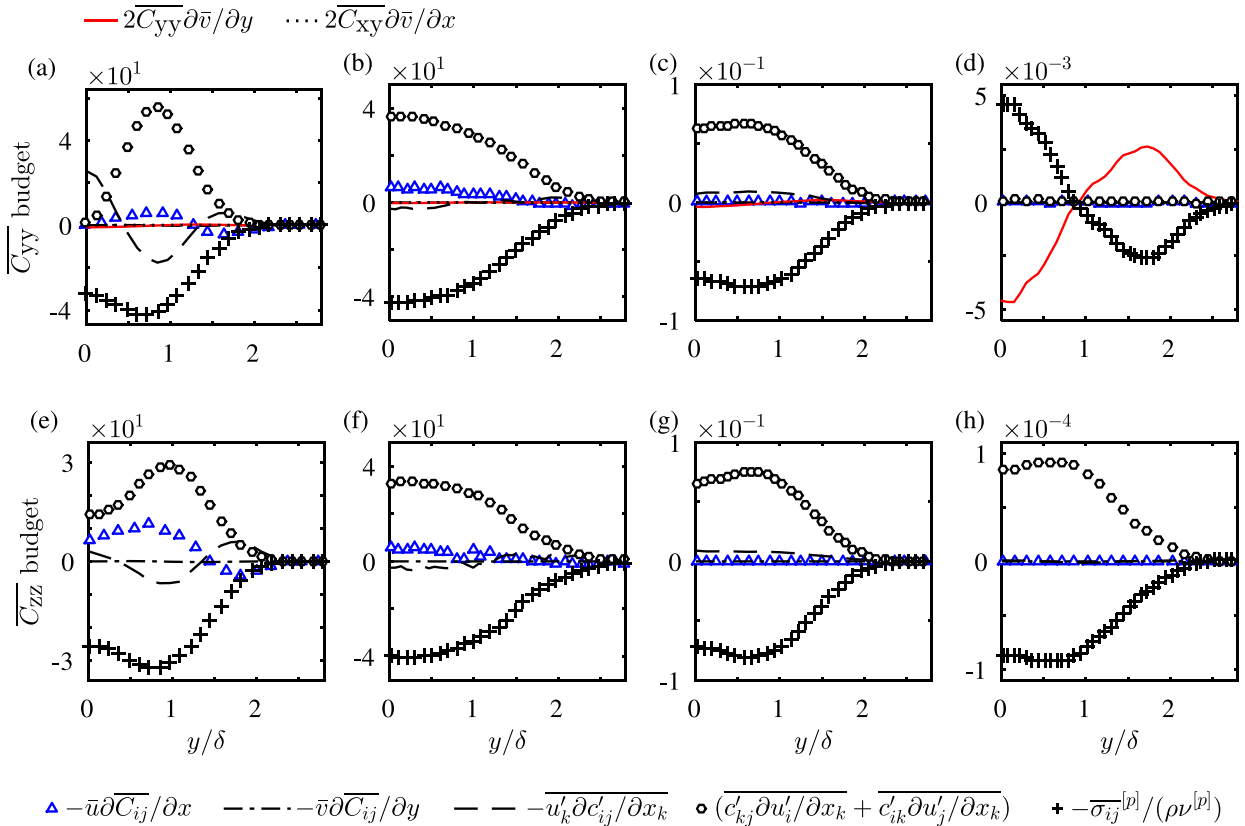


Fig. A.29. Budgets of \overline{C}_{yy} (a-d) and \overline{C}_{zz} (e-h) for wakes at different regimes of polymer chain deformation: (a,e) highly-stretched anisotropic, (b,f) highly-stretched nearly-isotropic, (c,g) nearly-coiled nearly-isotropic and (d,h) final region of decay. All quantities have been made non-dimensional using U_∞ and d . Flow conditions are: (a) and (e) $Re = 2000$, $Wi = 4$, $1 - \beta = 0.10$, $L = 100$, $x/d = 70$; (b) and (f) $Re = 2000$, $Wi = 3$, $1 - \beta = 0.02$, $L = 200$, $x/d = 180$; (c) and (g) $Re = 4000$, $Wi = 0.05$, $1 - \beta = 0.20$, $L = 100$, $x/d = 110$; (d) and (h) $Re = 1500$, $Wi = 0.0001$, $1 - \beta = 0.20$, $L = 100$, $x/d = 110$.

B.1. Planar wake

The balance equation for the trace \overline{C}_{ii} at the highly-stretching nearly-isotropic regime is

$$\begin{aligned}
 & \frac{De\delta}{f(c_{nn}+3)c_{ll}} \frac{U_\infty}{\Delta U} \frac{dc_{kk}}{dx} \left\{ g_{ii} \right\} - \\
 & \frac{De}{f(c_{nn}+3)} \frac{U_\infty}{\Delta U} \frac{d\delta^2}{dx} \left\{ \frac{1}{2} \frac{dg_{ii}}{d\xi} \xi \right\} - \frac{De\delta}{f(c_{nn}+3)c_{ll}} \frac{dc_{kk}}{dx} \\
 & \times \left\{ g_{ii}\psi \right\} - \frac{Dec_{xx}}{f(c_{nn}+3)c_{ll}\delta} \frac{d\delta^2}{dx} \left\{ g_{xx}\psi + \frac{d\psi}{d\xi} \xi g_{xx} \right\} \\
 & + \frac{Dec_{yy}}{f(c_{nn}+3)c_{ll}\delta} \frac{d\delta^2}{dx} \left\{ g_{yy}\psi + \frac{d\psi}{d\xi} \xi g_{yy} \right\} \\
 & - \frac{Dec_{xy}}{f(c_{nn}+3)c_{ll}\delta^2} \left(\frac{d\delta^2}{dx} \right)^2 \left\{ \frac{3}{2} g_{xy}\xi\psi + \frac{1}{2} g_{xy}\xi^2 \frac{d\psi}{d\xi} \right\} \\
 & + \frac{2Dec_{xy}}{f(c_{nn}+3)c_{ll}} \left\{ g_{xy} \frac{d\psi}{d\xi} \right\} \\
 & = \frac{\beta De^2 Re_\theta}{(1-\beta)2^{3/2} f(c_{nn}+3)^2 c_{ll}} A_{\delta^2}^{\frac{5}{4}} A_U^{\frac{1}{4}} \left\{ N_{ii} \right\} - \left\{ \sigma_{ii} \right\},
 \end{aligned} \tag{B.1}$$

and for the shear component \overline{C}_{xy} we have

$$\begin{aligned}
 & \frac{De\delta}{f(c_{nn}+3)c_{xy}} \frac{U_\infty}{\Delta U} \frac{dc_{xy}}{dx} \left\{ g_{xy} \right\} - \frac{De}{f(c_{nn}+3)} \left(\frac{U_\infty}{\Delta U} \right) \frac{d\delta^2}{dx} \\
 & \times \left\{ \frac{1}{2} \frac{dg_{xy}}{d\xi} \xi \right\} - \frac{De\delta}{f(c_{nn}+3)c_{xy}} \frac{dc_{xy}}{dx} \left\{ g_{xy}\psi \right\} \\
 & - \frac{Dec_{xx}}{f(c_{nn}+3)c_{xy}\delta^2} \left(\frac{d\delta^2}{dx} \right)^2 \left\{ \frac{3}{4} g_{xx}\xi\psi + \frac{1}{4} g_{xx}\xi^2 \frac{d\psi}{d\xi} \right\}
 \end{aligned}$$

$$\begin{aligned}
 & - \frac{De}{f(c_{nn}+3)c_{xy}\delta^2} \left(\frac{d\delta^2}{dx} \right)^2 \left\{ \frac{3}{4} \xi\psi + \frac{1}{4} \xi^2 \frac{d\psi}{d\xi} \right\} \\
 & - \frac{De}{f(c_{nn}+3)c_{xy}} \left\{ \frac{d\psi}{d\xi} \right\} \\
 & - \frac{Dec_{yy}}{f(c_{nn}+3)c_{xy}} \left\{ g_{yy} \frac{d\psi}{d\xi} \right\} = \left\{ N_{xy} \right\} - \left\{ \sigma_{xy} \right\}.
 \end{aligned} \tag{B.2}$$

For thin shear layers at very high Re the spreading rate normalized by the local half-width $[d\delta^2/dx]/\delta$ is small and so the 4th and 5th terms on the l.h.s. of (B.2) are negligible in comparison with the 7th and 6th terms, respectively. The 6th term is also much smaller than the 7th, because $c_{yy}(x) \gg 1$ at the highly stretched regime. For small velocity deficit wakes, $\Delta U/U_\infty \ll 1$ and so the 3rd term is much smaller than the first. For long chain polymers at the highly-stretched nearly-isotropic regime we have $c_{xx} \sim c_{yy} \sim c_{zz} \sim c_{ll}/3 \gg 1$, the local Deborah number $De(x)$ has order unity and $1/f(c_{ll}+3)$ is small. Using this and assuming a general power law that decays in x for $c_{xy}(x)$, in order to evaluate $dc_{xy}(x)/dx$, and the scaling laws for $\delta(x)$ and $\Delta U(x)$, one finds that the first term on the l.h.s. is much smaller than the dominant terms of order unity, because x is large at the far field. Using the momentum integral constraint to evaluate the 2nd term and considering again that the spreading rate parameter is small for thin shear layers the 2nd term is found to be also much smaller than unity. Therefore, the only terms left are those on the last line of Eq. (B.2) and the simplified Eq. (28) is obtained.

If similar arguments are applied to Eq. (B.1) for the trace \overline{C}_{ii} , the simplified Eq. (29) is obtained from (B.1) when we use the similarity condition of the \overline{C}_{xy} equation, $Dec_{yy}/[f(c_{nn}+3)c_{xy}] \sim 1$, to estimate the order of $c_{xy}(x)$ in terms of the remaining quantities, and also that for dilute polymer solutions $\beta/(1-\beta)$ is large and the inlet Reynolds number

Re_θ is large. The equations for each normal component of $\overline{C_{ij}}(x, y)$ can be analysed in the same manner, leading to similar results.

We now consider the polymers at the nearly-coiled sub-regimes. Using the self-similarity transformations developed for the nearly-coiled regimes we obtain

$$\begin{aligned} De \frac{U_\infty}{\Delta U} \frac{\delta}{c_{yy}} \frac{dc_{xy}}{dx} \left\{ g_{xy} \right\} - \frac{De}{c_{yy}} c_{xy} \left(\frac{U_\infty}{\Delta U \delta} \right) \frac{d\delta^2}{dx} \left\{ \frac{1}{2} \frac{dg_{xy}}{d\xi} \xi \right\} \\ - \frac{De}{c_{yy}} \frac{c_{xx}}{\delta^2} \left(\frac{d\delta^2}{dx} \right)^2 \left\{ \frac{3}{4} g_{xx} \xi \psi + \frac{1}{4} g_{xx} \xi^2 \frac{d\psi}{d\xi} \right\} - \\ De \frac{\delta}{c_{yy}} \frac{dc_{xy}}{dx} \left\{ g_{xy} \psi \right\} - \frac{De}{c_{yy}} \frac{1}{\delta^2} \left(\frac{d\delta^2}{dx} \right)^2 \left\{ \frac{3}{4} \xi \psi + \frac{1}{4} \xi^2 \frac{d\psi}{d\xi} \right\} - \\ \frac{De}{c_{yy}} \left\{ \frac{d\psi}{d\xi} \right\} - De \left\{ g_{yy} \frac{d\psi}{d\xi} \right\} = \frac{1}{\theta} \frac{d\delta^2}{dx} \left\{ N_{xy} \right\} - \frac{c_{xy}}{c_{yy}} \left\{ \sigma_{xy} \right\}, \end{aligned} \quad (B.3)$$

for $\overline{C_{xy}}$,

$$\begin{aligned} De \frac{U_\infty}{\Delta U} \frac{\delta}{c_{xx}} \frac{dc_{xx}}{dx} \left\{ g_{xx} \right\} - De \left(\frac{U_\infty}{\Delta U \delta} \right) \frac{d\delta^2}{dx} \left\{ \frac{1}{2} \frac{dg_{xx}}{d\xi} \xi \right\} \\ - De \frac{1}{\delta} \frac{d\delta^2}{dx} \left\{ g_{xx} \psi + \frac{d\psi}{d\xi} \xi g_{xx} \right\} - \frac{De}{c_{xx}} \frac{1}{\delta} \frac{d\delta^2}{dx} \left\{ \psi + \frac{d\psi}{d\xi} \xi \right\} \\ - De \frac{\delta}{c_{xx}} \frac{dc_{xx}}{dx} \left\{ g_{xx} \psi \right\} + \frac{De}{c_{xx}} c_{xy} \left\{ 2g_{xy} \frac{d\psi}{d\xi} \right\} \\ = \frac{\beta De^2 Re_\theta A_\delta^{5/4} A_{\Delta U}^{1/4}}{3\sqrt{8}c_{xx}} \left\{ N_{xx} \right\} - \left\{ \sigma_{xx} \right\}, \end{aligned} \quad (B.4)$$

for $\overline{C_{xx}}$,

$$\begin{aligned} De \frac{U_\infty}{\Delta U} \frac{\delta}{c_{yy}} \frac{dc_{yy}}{dx} \left\{ g_{yy} \right\} - De \left(\frac{U_\infty}{\Delta U \delta} \right) \frac{d\delta^2}{dx} \left\{ \frac{1}{2} \frac{dg_{yy}}{d\xi} \xi \right\} \\ + De \frac{1}{\delta} \frac{d\delta^2}{dx} \left\{ g_{yy} \psi + \frac{d\psi}{d\xi} \xi g_{yy} \right\} + \frac{De}{c_{yy}} \frac{1}{\delta} \frac{d\delta^2}{dx} \left\{ \psi + \frac{d\psi}{d\xi} \xi \right\} \\ - \frac{De}{c_{yy}} \frac{c_{xy}}{\delta^2} \left(\frac{d\delta^2}{dx} \right)^2 \left\{ \frac{3}{2} g_{xy} \xi \psi + \frac{1}{2} g_{xy} \xi^2 \frac{d\psi}{d\xi} \right\} - De \frac{\delta}{c_{yy}} \frac{dc_{yy}}{dx} \\ \times \left\{ g_{yy} \psi \right\} = \frac{\beta De^2 Re_\theta A_\delta^{5/4} A_{\Delta U}^{1/4}}{3\sqrt{8}c_{yy}} \left\{ N_{yy} \right\} - \left\{ \sigma_{yy} \right\}, \end{aligned} \quad (B.5)$$

for $\overline{C_{yy}}$ and finally

$$\begin{aligned} De \frac{U_\infty}{\Delta U} \frac{\delta}{c_{zz}} \frac{dc_{zz}}{dx} \left\{ g_{zz} \right\} - De \left(\frac{U_\infty}{\Delta U \delta} \right) \frac{d\delta^2}{dx} \left\{ \frac{1}{2} \frac{dg_{zz}}{d\xi} \xi \right\} \\ - De \frac{\delta}{c_{zz}} \frac{dc_{zz}}{dx} \left\{ g_{zz} \psi \right\} \\ = \frac{\beta De^2 Re_\theta A_\delta^{5/4} A_{\Delta U}^{1/4}}{3\sqrt{8}c_{zz}} \left\{ N_{zz} \right\} - \left\{ \sigma_{zz} \right\}, \end{aligned} \quad (B.6)$$

for $\overline{C_{zz}}$. The analysis is very similar to that of the highly-stretched regime, but at the nearly-coiled nearly-isotropic regime we have $c_{xx}(x) \sim c_{yy}(x) \sim c_{zz}(x) \sim c_{il}(x)/3 \ll 1$ and the local Deborah number $De(x)$ is low. The treatment of the $\overline{C_{xy}}$ and $\overline{C_{zz}}$ equations is then straightforward, but the $\overline{C_{xx}}$ and $\overline{C_{yy}}$ equations require a closer examination. Under the limiting case in consideration they reduce to

$$\begin{aligned} \pm \frac{De}{c_{xx,yy}} \frac{d\delta^2}{dx} \left\{ \psi + \xi \frac{d\psi}{d\xi} \right\} + \\ \frac{\beta De^2 Re_\theta A_\delta^{5/4} A_{\Delta U}^{1/4}}{3\sqrt{8}c_{xx,yy}} \left\{ N_{xx,yy} \right\} = \left\{ \sigma_{xx,yy} \right\} \end{aligned} \quad (B.7)$$

Performing some algebraic manipulations on Eq. (B.7), and using the scaling law for $\Delta U(x)$, Eq. (B.7) can be written as

$$\begin{aligned} \pm \frac{De}{c_{xx,yy}} \frac{d\delta^2}{dx} \left\{ \psi + \xi \frac{d\psi}{d\xi} \right\} + \\ \frac{De}{c_{xx,yy}} \frac{d\delta^2}{dx} \left(\frac{\beta Wi_\theta Re_\theta A_\delta^{1/4} A_{\Delta U}^{-1/4}}{3\sqrt{8}\sqrt{(x-x_0)/\theta}} \right) \left\{ N_{xx,yy} \right\} = \left\{ \sigma_{xx,yy} \right\}. \end{aligned} \quad (B.8)$$

Eq. (B.8) contains the simplified balance equations of the nearly-coiled nearly-isotropic sub-regime and nearly-coiled final region of decay as particular cases. To show that, we analyse the term inside parenthesis. At regions where

$$\frac{x-x_0}{\theta} \ll \left(\frac{\beta Wi_\theta Re_\theta A_\delta^{1/4} A_{\Delta U}^{-1/4}}{3\sqrt{8}} \right)^2 \quad (B.9)$$

the term inside parenthesis is much larger than one, so the first term on the l.h.s. of Eq. (B.8) is negligibly small in comparison to the second, and the balance equation of the nearly-coiled nearly-isotropic sub-regime is recovered. For more distant regions where

$$\frac{x-x_0}{\theta} \gg \left(\frac{\beta Wi_\theta Re_\theta A_\delta^{1/4} A_{\Delta U}^{-1/4}}{3\sqrt{8}} \right)^2, \quad (B.10)$$

the term inside parenthesis in Eq. (B.8) is much smaller than one, the second term on the l.h.s. of Eq. (B.8) is negligibly small in comparison to the first, and the balance equation of the nearly-coiled final region of decay is recovered.

B.2. Planar jet

As mentioned at Section 6 the asymptotic analysis of the turbulent planar jet equations is similar to that of the planar wake, so we only show the self-similarity equations without giving many details. At the highly-stretched nearly-coiled regime the equation for the trace $\overline{C_{ii}}$ is

$$\begin{aligned} \frac{De\delta}{f(c_{nn}+3)c_{il}} \frac{dc_{kk}}{dx} \left\{ \psi g_{ii} \right\} - \frac{De}{f(c_{nn}+3)} \frac{d\delta}{dx} \\ \times \left\{ \frac{dg_{ii}}{d\xi} \int_0^\xi \frac{\psi}{2} d\tilde{\xi} - \frac{2Dec_{xy}}{f(c_{nn}+3)c_{ii}} \left\{ g_{xy} \frac{d\psi}{d\xi} \right\} \right\} \\ - \frac{Dec_{yy}}{f(c_{nn}+3)c_{ii}} \frac{d\delta}{dx} \left\{ \psi g_{yy} + 2g_{yy} \xi \frac{d\psi}{d\xi} \right\} + \frac{Dec_{xx}}{f(c_{nn}+3)c_{ii}} \frac{d\delta}{dx} \\ \times \left\{ \psi g_{xx} + 2g_{xx} \xi \frac{d\psi}{d\xi} \right\} + \frac{Dec_{xy}}{f(c_{nn}+3)c_{ii}} \left(\frac{d\delta}{dx} \right)^2 \\ \times \left\{ g_{xy} \int_0^\xi \left[\frac{3}{2} \psi + 6\tilde{\xi} \frac{d\psi}{d\tilde{\xi}} + 2\tilde{\xi}^2 \frac{d^2\psi}{d\tilde{\xi}^2} \right] d\tilde{\xi} \right\} \\ = \frac{\beta De^2 Re_\theta}{(1-\beta)f(c_{nn}+3)^2 c_{il}} \left(\frac{d\delta}{dx} \right)^{\frac{3}{2}} \left\{ N_{ii} \right\} - \left\{ \sigma_{ii} \right\}, \end{aligned} \quad (B.11)$$

while for the shear component $\overline{C_{xy}}$ we have.

$$\begin{aligned} \frac{A_\delta De\delta}{f(c_{ii}+3)c_{xy}} \frac{dc_{xy}}{dx} \left\{ \psi g_{xy} \right\} - \frac{A_\delta De}{f(c_{ii}+3)} \frac{d\delta}{dx} \\ \times \left\{ \frac{dg_{xy}}{d\xi} \int_0^\xi \frac{\psi}{2} d\tilde{\xi} \right\} + \frac{A_\delta Dec_{xx}}{f(c_{ii}+3)c_{xy}} \left(\frac{d\delta}{dx} \right)^2 \\ \times \left\{ g_{xx} \int_0^\xi \left[\frac{3}{4} \psi + 3\tilde{\xi} \frac{d\psi}{d\tilde{\xi}} + \tilde{\xi}^2 \frac{d^2\psi}{d\tilde{\xi}^2} \right] d\tilde{\xi} \right\} \\ + \frac{A_\delta De}{f(c_{ii}+3)c_{xy}} \left(\frac{d\delta}{dx} \right)^2 \left\{ \int_0^\xi \left[\frac{3}{4} \psi + 3\tilde{\xi} \frac{d\psi}{d\tilde{\xi}} + \tilde{\xi}^2 \frac{d^2\psi}{d\tilde{\xi}^2} \right] d\tilde{\xi} \right\} \\ - \frac{A_\delta De}{f(c_{ii}+3)c_{xy}} \left\{ \frac{d\psi}{d\xi} \right\} \\ - \frac{A_\delta Dec_{yy}}{f(c_{ii}+3)c_{xy}} \left\{ g_{yy} \frac{d\psi}{d\xi} \right\} = \left\{ N_{xy} \right\} - A_\delta \left\{ \sigma_{xy} \right\}. \end{aligned} \quad (B.12)$$

As for the planar wake configuration, these equations also reduce to the simplified Eqs. (20) and (21), but for the planar jet the small parameter is the constant spreading rate $A_\delta = d\delta/dx$. For the shear component, the relaxation term can also be neglected which leads to an equation similar to Eq. (20) but without the relaxation term.

With the self-similarity transformations developed for the nearly-coiled regimes the self-similarity equations are

$$\begin{aligned} De \frac{\delta}{c_{yy}} \frac{dc_{xy}}{dx} \left\{ \psi g_{xy} \right\} + \frac{De}{c_{yy}} c_{xy} \frac{d\delta}{dx} \left\{ -\frac{dg_{xy}}{d\xi} \int_0^\xi \frac{\psi}{2} d\tilde{\xi} \right\} \\ + De \left\{ -g_{yy} \frac{d\psi}{d\xi} \right\} + \frac{De}{c_{yy}} \left\{ -\frac{d\psi}{d\xi} \right\} + \frac{De}{c_{yy}} c_{xx} \left(\frac{d\delta}{dx} \right)^2 \\ \times \left\{ g_{xx} \int_0^\xi \left[\frac{3}{4} \psi + 3\tilde{\xi} \frac{d\psi}{d\tilde{\xi}} + \tilde{\xi}^2 \frac{d^2\psi}{d\tilde{\xi}^2} \right] d\tilde{\xi} \right\} \\ + \frac{De}{c_{yy}} \left(\frac{d\delta}{dx} \right)^2 \left\{ \int_0^\xi \left[\frac{3}{4} \psi + 3\tilde{\xi} \frac{d\psi}{d\tilde{\xi}} + \tilde{\xi}^2 \frac{d^2\psi}{d\tilde{\xi}^2} \right] d\tilde{\xi} \right\} \\ = \frac{d\delta}{dx} \left\{ N_{xy} \right\} - \frac{c_{xy}}{c_{yy}} \left\{ \sigma_{xy} \right\}, \end{aligned} \quad (\text{B.13})$$

for the $\overline{C_{xy}}$ component,

$$\begin{aligned} De \frac{\delta}{c_{xx}} \frac{dc_{xx}}{dx} \left\{ \psi g_{xx} \right\} + \frac{De}{c_{xx}} \frac{d\delta}{dx} \left\{ \psi + 2\xi \frac{d\psi}{d\xi} \right\} \\ + De \frac{d\delta}{dx} \left\{ -\frac{dg_{xx}}{d\xi} \int_0^\xi \frac{\psi}{2} d\tilde{\xi} + g_{xx}\psi + 2g_{xx}\xi \frac{d\psi}{d\xi} \right\} + \\ \frac{De}{c_{xx}} c_{xy} \left\{ -2g_{xy} \frac{d\psi}{d\xi} \right\} = \frac{\beta De^2 Re_\delta A_\delta^{3/2}}{3c_{xx}} \left\{ N_{xx} \right\} - \left\{ \sigma_{xx} \right\}, \end{aligned} \quad (\text{B.14})$$

for $\overline{C_{xx}}$,

$$\begin{aligned} De \frac{\delta}{c_{yy}} \frac{dc_{yy}}{dx} \left\{ \psi g_{yy} \right\} - \frac{De}{c_{yy}} \frac{d\delta}{dx} \left\{ \psi + 2\xi \frac{d\psi}{d\xi} \right\} \\ + De \frac{d\delta}{dx} \left\{ -\frac{dg_{yy}}{d\xi} \int_0^\xi \frac{\psi}{2} d\tilde{\xi} - g_{yy}\psi - 2g_{yy}\xi \frac{d\psi}{d\xi} \right\} \\ + \frac{De}{c_{yy}} c_{xy} \left(\frac{d\delta}{dx} \right)^2 \left\{ g_{xy} \int_0^\xi \left[\frac{3}{2} \psi + 6\tilde{\xi} \frac{d\psi}{d\tilde{\xi}} + 2\tilde{\xi}^2 \frac{d^2\psi}{d\tilde{\xi}^2} \right] d\tilde{\xi} \right\} \\ = \frac{\beta De^2 Re_\delta A_\delta^{3/2}}{3c_{yy}} \left\{ N_{yy} \right\} - \left\{ \sigma_{yy} \right\}, \end{aligned} \quad (\text{B.15})$$

for $\overline{C_{yy}}$ and

$$\begin{aligned} De \frac{\delta}{c_{zz}} \frac{dc_{zz}}{dx} \left\{ \psi g_{zz} \right\} - De \frac{d\delta}{dx} \left\{ \frac{dg_{zz}}{d\xi} \int_0^\xi \frac{\psi}{2} d\tilde{\xi} \right\} \\ = \frac{\beta De^2 Re_\delta A_\delta^{3/2}}{3c_{zz}} \left\{ N_{zz} \right\} - \left\{ \sigma_{zz} \right\}, \end{aligned} \quad (\text{B.16})$$

for $\overline{C_{zz}}$. At the asymptotic limit of the nearly-coiled regimes the equations for $\overline{C_{xx}}$ and $\overline{C_{yy}}$ reduce to

$$\begin{aligned} \mp \frac{De}{c_{xx,yy}} \frac{d\delta}{dx} \left\{ \psi + 2\xi \frac{d\psi}{d\xi} \right\} \\ + \frac{\beta De^2 Re_\delta A_\delta^{3/2}}{c_{xx,yy}} \left\{ N_{xx,yy} \right\} = \left\{ \sigma_{xx,yy} \right\}, \end{aligned} \quad (\text{B.17})$$

which can be written as

$$\begin{aligned} \mp \frac{De}{c_{xx,yy}} \frac{d\delta}{dx} \left\{ \psi + 2\xi \frac{d\psi}{d\xi} \right\} \\ + \frac{De}{c_{xx,yy}} \frac{d\delta}{dx} \left(\frac{\beta Wi Re A_{U_c}^{-1} A_\delta^{1/2}}{(x-x_0)/h} \right) \left\{ N_{xx,yy} \right\} = \left\{ \sigma_{xx,yy} \right\}, \end{aligned} \quad (\text{B.18})$$

after using the definitions of $De(x)$, $Re_\delta(x)$ and the scaling laws for $\delta(x)$ and $U_c(x)$. For the regions where

$$\frac{x-x_0}{h} \ll \beta Wi Re A_{U_c}^{-1} A_\delta^{1/2}, \quad (\text{B.19})$$

the term inside parenthesis in Eq. (B.18) is much larger than one and the first term on the l.h.s. of the same equation is much smaller than the second, and the equation reduces to the simplified balance equation of the nearly-coiled nearly-isotropic regime. For more distant regions where

$$\frac{x-x_0}{h} \gg \beta Wi Re A_{U_c}^{-1} A_\delta^{1/2}, \quad (\text{B.20})$$

the term inside parenthesis in Eq. (B.18) is much smaller than one and the second term on the l.h.s. of Eq. (B.18) is much smaller than the first term, and the equation reduces to the simplified balance equation of the nearly-coiled final region of decay.

Appendix C. Domain of validity

Here we discuss the domain of validity of the different scaling laws in terms of the non-dimensional characteristic length scales $\ell_{c_{ij},1}$, $\ell_{c_{ij},2}$ and $\ell_{c_{ij},3}$ as shown in Fig. 26, where we use d and h to normalize these length scales, for wakes and jets, respectively. As demonstrated below, these characteristic length scales depend on the component of the conformation tensor under analysis. We start with $\ell_{c_{ij},3}$ and $\ell_{c_{ij},2}$ because analytical formulas can be derived for them. A numerical procedure is indicated for the calculation of $\ell_{c_{ij},1}$ at the end of this appendix.

The upper boundaries $\ell_{c_{xx},3}$ and $\ell_{c_{yy},3}$ demarcating the transition between the nearly-coiled nearly-isotropic and nearly-coiled final region of decay sub-regimes for the $\overline{C_{xx}}$ and $\overline{C_{yy}}$ components, respectively, are the most straightforward to obtain. The transition is when the validity of the condition given by the inequalities (B.9), for wakes, and (B.19), for jets, ceases. The results obtained for the planar wake are given by

$$\ell_{c_{xx},3} = \ell_{c_{yy},3} = \gamma_1 (\beta Wi_\theta Re_\theta)^2. \quad (\text{C.1})$$

and for the planar jet they are

$$\ell_{c_{xx},3} = \ell_{c_{yy},3} = \gamma_1 \beta Wi Re. \quad (\text{C.2})$$

The γ_i coefficients were introduced so that we can write the equations with a more compact notation that emphasizes the functional dependences on the more important parameters: β , Wi and Re . Their definitions and calculated values are given at Table C.2. Some γ_i have a non-unitary order of magnitude, so they need to be kept in the formulation.

Notice that for components $\overline{C_{zz}}$ and $\overline{C_{xy}}$ and trace $\overline{C_{ii}}$ the simplified governing equations and the resulting scaling laws are the same at the nearly-coiled nearly-isotropic sub-regime and final region of decay, so that $\ell_{c_{zz},3} = \ell_{c_{xy},3} = \ell_{c_{ii},3} \rightarrow \infty$.

The non-dimensional length scales $\ell_{c_{ij},2}$ marking the transition between the highly-stretched and nearly-coiled sub-regimes are obtained by imposing that each negligible term of the $\overline{C_{ij}}$ equation at the nearly-coiled nearly-isotropic regime is much smaller than the dominant terms of the equation. For example, in Eq. (B.14) it was found that the advection term of order $De(\delta/c_{xx})dc_{xx}/dx$ is much smaller than the dominant terms of order unity, i.e. $|De(\delta/c_{xx})dc_{xx}/dx| \ll 1$. Substitution of the scaling laws for $De(x)$, $\delta(x)$ and $c_{xx}(x)$ at the nearly-coiled nearly-isotropic regime gives $(5/2)Wi A_{U_c}^{-1/2} [(x-x_0)/h]^{-3/2} \ll 1$, which can be re-written as $(x-x_0)/h \gg Wi^{2/3} [(5/2)^{2/3} A_{U_c}^{-1/3}]$ so that $\ell_{c_{ij},2} = Wi^{2/3} [(5/2)^{2/3} A_{U_c}^{-1/3}]$. Doing similarly to another negligible term of the same equation gives $\ell_{c_{ij},2} = \gamma_3 \beta^{-2} Re^{-2}$. This procedure is carried out for all components of $\overline{C_{ij}}$ and its trace, leading to the following results for a planar jet

$$\ell_{c_{xx},2} = \max\{\gamma_2 Wi^{2/3}, \gamma_3 \beta^{-2} Re^{-2}\}, \quad (\text{C.3})$$

$$\ell_{c_{yy},2} = \max\{\gamma_2 Wi^{2/3}, \gamma_4 \beta^{-2} Re^{-2}\}, \quad (\text{C.4})$$

$$\ell_{c_{zz},2} = \gamma_2 Wi^{2/3}, \quad (\text{C.5})$$

$$\ell_{c_{xy},2} = \max\{(3/5)^{2/3} \gamma_2 Wi^{2/3}, \gamma_5 \beta Wi Re\}, \quad (\text{C.6})$$

$$\ell_{c_{ii},2} = \max\{\gamma_2 Wi^{2/3}, \gamma_3 \beta^{-2} Re^{-2}\}. \quad (\text{C.7})$$

The results for the planar wake are

$$\ell_{c_{xx},2} = \max\{\gamma_2 Wi_\theta^{2/3}, 2Wi_\theta\}, \quad (\text{C.8})$$

Table C.2Definitions and calculated values for the γ_i coefficients appearing in the expressions for the characteristic distances $\ell_{c_{ij},2}$ and $\ell_{c_{ij},3}$.

Coefficients	γ_1	γ_2	γ_3	γ_4	γ_5
Definition (wakes)	$\left(\frac{A_{\delta}^{1/4} A_{\Delta U}^{-1/4}}{3\sqrt{8}}\right)^2$	$\frac{2^{2/3}}{A_{\Delta U}^{1/3}}$	$\frac{A_{\Delta U}^{-1/4} A_{c_{xy}}^2}{A_{\delta}^{9/4} A_{c_{xy}}}$	$\frac{A_{\delta}^{9/8} A_{c_{xy}}^{1/2}}{A_{\Delta U}^{3/8} A_{c_{xy}}}$	$\frac{A_{\delta}^{15/4} A_{c_{xy}}}{A_{\Delta U}^{1/4} A_{c_{xy}}^2}$
Numerical value (wakes)	0.007	2.5	12.7	0.54	0.003
Definition (jets)	$\frac{A_{\delta}^{1/2}}{A_{U_c}}$	$\frac{(5/2)^{2/3}}{A_{U_c}^{1/3}}$	$\frac{A_{U_c} A_{c_{xx}}^3}{A_{\delta}^3 A_{c_{xy}}^3}$	$\frac{A_{U_c} A_{c_{xy}}^3}{A_{\delta}^3 A_{c_{xy}}^3}$	$\frac{A_{\delta}^{5/2} A_{c_{xy}}^{3/2}}{A_{U_c} A_{c_{xy}}^{5/2}}$
Numerical value (jets)	1.8	3.3	5.7×10^5	25	0.003

$$\ell_{c_{yy},2} = \max\{\gamma_2 Wi_{\theta}^{2/3}, 2Wi_{\theta}, \gamma_3 \beta^{-1} Re_{\theta}^{-1}\}, \quad (C.9)$$

$$\ell_{c_{zz},2} = \max\{\gamma_2 Wi_{\theta}^{2/3}, 2Wi_{\theta}\}, \quad (C.10)$$

$$\ell_{c_{xy},2} = \max\{\gamma_2 Wi_{\theta}^{2/3}, j^{2/3}, Wi_{\theta}, \gamma_4 Wi_{\theta} (\beta Re_{\theta})^{1/2}, \gamma_5 \beta Wi_{\theta} Re_{\theta}\}, \quad (C.11)$$

$$\ell_{c_{ii},2} = \max\{\gamma_1 Wi_{\theta}^{2/3}, 2Wi_{\theta}\}. \quad (C.12)$$

For both jets and wakes a $Wi^{2/3}$ scaling appears for $\ell_{c_{ij},2}$, whereas a Wi or Wi_{θ}^2 scaling, for jets or wakes, appears for $\ell_{c_{xx},3}$ and $\ell_{c_{yy},3}$. The influence of the inlet Reynolds number and β also appears in the inequalities. Considering that Re is much larger than Wi and also that Re is sufficiently large, the $\ell_{c_{xy},2}$ formula indicates a linear variation with Re for both jets and wakes. $\ell_{c_{xx},3}$ and $\ell_{c_{yy},3}$ also vary linearly with Re for jets, but exhibit a quadratic Re_{θ}^2 growth for wakes. These conclusions are true for the asymptotic limit $Re \rightarrow \infty$, but when Re is not sufficiently high the terms involving e.g. $\gamma_3 \beta^{-2} Re^{-2}$, for the $\ell_{c_{xx},2}$ of jets, might actually dominate because the coefficient $\gamma_3 \sim 10^5$ is large.

To calculate $\ell_{c_{ij},1}$ we have to consider the scaling laws and corresponding self-similarity equations at the highly-stretched nearly-isotropic regime of polymer deformation. If we follow a procedure analogous to that described above for the calculation of $\ell_{c_{ij},2}$ but adapted to the highly-stretched nearly-isotropic regime, we obtain the equations for each $\ell_{c_{ij},1}$ length scale. Since the scaling laws at the highly-stretched regime are more complex than those of the nearly-coiled regime, the resulting equations for $\ell_{c_{ij},1}$ are non-linear, and can only be solved numerically. Even though these numerical solutions can be useful, for example, to evaluate composite expansions, they do not lead to further insights in terms of the flow physics and thus will not be presented here for brevity.

Appendix D. Derivation of the transverse profiles of the normalized conformation tensor $g_{ij}(\xi)$

D.1. Planar wake

The adopted intermittency model assumes a velocity jump over an infinitely thin turbulent interface whose position with respect to the flow centreline has a Gaussian distribution with mean $\mu \times \delta(x)$ and standard deviation $\sigma \times \delta(x)$. A convolution integral leads to the formula for the mean profile [34]

$$\bar{u} = \gamma_s u_{turb} + (1 - \gamma_s) u_{pot}, \quad (D.1)$$

where $u_{turb}(x, y) = U_{\infty} - \Delta U(x) \tilde{\psi}(\xi)$ is the mean velocity obtained from mixing length theory without any intermittency correction, $u_{pot} = U_{\infty}$ is the potential velocity and the intermittency factor follows a self-similar downstream development described by [34,39,40]

$$\gamma_s(\xi) = \frac{1}{2} \left[1 - \operatorname{erf}\left(\frac{\xi - \mu}{\sqrt{2}\sigma}\right) \right]. \quad (D.2)$$

The turbulent planar wake profile $\tilde{\psi}(\xi)$ (the tilde indicates the function without the intermittency correction) was obtained originally by Schlichting (1930) [3] and later by Görtler (1942) [4] and others. The formula adopted here is also derived at Pope (2000) [8]:

$$\tilde{\psi}(\xi) = \exp(-\alpha \xi^2) \quad (D.3)$$

where $\alpha = \ln 2$. Combining (D.3) with the intermittency model described above, $\psi(\xi)$ is obtained, and substitution of the result into Eqs. (37) and (41) leads to

$$g_{xy}(\xi) = -\chi_{c_{xy}} \exp(-\alpha \xi^2) \times \left\{ \alpha \xi \left[1 - \operatorname{erf}\left(\frac{\xi - \mu}{\sqrt{2}\sigma}\right) \right] + \frac{\exp\left[\frac{-(\xi - \mu)^2}{2\sigma^2}\right]}{\sqrt{2\pi}\sigma} \right\}, \quad (D.4)$$

$$g_{xx}(\xi) = \chi_{c_{xx}} \exp(-\alpha \xi^2) \times \left\{ \left[\frac{1}{2} - \alpha \xi^2 \right] \left[1 - \operatorname{erf}\left(\frac{\xi - \mu}{\sqrt{2}\sigma}\right) \right] - \xi \frac{\exp\left[\frac{-(\xi - \mu)^2}{2\sigma^2}\right]}{\sqrt{2\pi}\sigma} \right\}, \quad (D.5)$$

$$g_{yy}(\xi) = -g_{xx}(\xi). \quad (D.6)$$

The model parameters $\chi_{c_{ij}}$ are calculated by taking the maximum value of the functions that appear on each side of the corresponding $g_{ij}(\xi)$ equations, isolating $\chi_{c_{ij}}$ and using the limit value of the function ($\max[g_{ij}(\xi)] = 1$). For example, for the shear component we have

$$\chi_{c_{xy}} = \max|g_{xy}(\xi)| / \max \left| \exp(-\alpha \xi^2) \left\{ \alpha \xi \left[1 - \operatorname{erf}\left(\frac{\xi - \mu}{\sqrt{2}\sigma}\right) \right] + \frac{\exp\left[\frac{-(\xi - \mu)^2}{2\sigma^2}\right]}{\sqrt{2\pi}\sigma} \right\} \right| \quad (D.7)$$

where $\max|g_{xy}(\xi)| = 1$.

After a linearization (explained below), the balance equation for κ written with similarity variables ($K = \kappa / u'^2$) is

$$\frac{d^2 K}{d\xi^2} + B_1 \frac{dK}{d\xi} + C_1 K = D_1 \left(\frac{d\psi}{d\xi} \right)^2, \quad (D.8)$$

with boundary conditions given by

$$K(\xi = 0) = K_0, \quad K(\xi \rightarrow \infty) = 0, \quad (D.9)$$

where we have introduced some non-dimensional, constant coefficients to simplify the notation. The equation coefficients are given by

$$B_1 = \frac{\sqrt{2} A_{\sigma} A_{\Delta U}^{1/4} A_{\delta}^{1/4}}{2\tilde{v}_t}, \quad D_1 = \frac{-2A_{\sigma}}{A_{\Delta U}^{1/2} A_{\delta}^{1/2}}, \quad (D.10)$$

$$C_1 = \frac{\sqrt{2} A_{\sigma} A_{\Delta U}^{1/4} A_{\delta}^{1/4} - A_{\epsilon} A_{\sigma} \sqrt{K_0}}{\tilde{v}_t}. \quad (D.11)$$

The ordinary differential equation (ODE) for $K(\xi)$ is actually non-linear and we arrived at Eq. (D.8) after a linearization of the ODE using the following approximation

$$K^{3/2} = \sqrt{K} K \approx \sqrt{K_0} K. \quad (D.12)$$

Therefore, Eq. (D.8) is a second order inhomogeneous ODE with constant coefficients whose general solution can be obtained from the

method of variation of parameters. The solution depends on the sign of the discriminant of the equation, Δ , which is

$$\Delta = B_1^2 - 4C_1. \quad (\text{D.13})$$

Since Δ is always positive, the general solution of the ODE for the wake is

$$\begin{aligned} K(\xi) = & \widetilde{C}_1 \exp\left\{-\frac{\xi}{2}(B_1 + \sqrt{\Delta})\right\} + \\ & \widetilde{C}_2 \exp\left\{-\frac{\xi}{2}(B_1 - \sqrt{\Delta})\right\} + \frac{D_1}{4} \exp\{-2\alpha\xi^2\} \\ & + \frac{D_1 \sqrt{\pi/2}}{32\sqrt{\alpha\Delta}} [16\alpha + (B_1 + \sqrt{\Delta})^2] \times \\ & \exp\left\{\frac{-16\alpha\xi(B_1 + \sqrt{\Delta}) + (B_1 + \sqrt{\Delta})^2}{32\alpha}\right\} \\ & \times \operatorname{erf}\left\{\frac{-8\alpha\xi + B_1 + \sqrt{\Delta}}{4\sqrt{2\alpha}}\right\} \\ & + \frac{D_1 \sqrt{\pi/2}}{32\sqrt{\alpha\Delta}} [16\alpha + (B_1 - \sqrt{\Delta})^2] \times \\ & \exp\left\{\frac{-16\alpha\xi(B_1 - \sqrt{\Delta}) + (B_1 - \sqrt{\Delta})^2}{32\alpha}\right\} \\ & \times \operatorname{erf}\left\{\frac{8\alpha\xi - B_1 + \sqrt{\Delta}}{4\sqrt{2\alpha}}\right\}, \end{aligned} \quad (\text{D.14})$$

where the integration constants \widetilde{C}_1 and \widetilde{C}_2 are specified by the boundary conditions and are given by

$$\widetilde{C}_2 = -\frac{D_1 \sqrt{\pi/2}}{32\sqrt{\alpha\Delta}} [16\alpha + (B_1 - \sqrt{\Delta})^2] \exp\left\{\frac{(B_1 - \sqrt{\Delta})^2}{32\alpha}\right\} \quad (\text{D.15})$$

and

$$\begin{aligned} \widetilde{C}_1 = & K_0 - \frac{D_1}{4} - \frac{D_1 \sqrt{\pi/2}}{32\sqrt{\alpha\Delta}} [16\alpha + (B_1 + \sqrt{\Delta})^2] \times \\ & \exp\left\{\frac{(B_1 + \sqrt{\Delta})^2}{32\alpha}\right\} \operatorname{erf}\left\{\frac{B_1 + \sqrt{\Delta}}{4\sqrt{2\alpha}}\right\} \\ & - \frac{D_1 \sqrt{\pi/2}}{32\sqrt{\alpha\Delta}} [16\alpha + (B_1 - \sqrt{\Delta})^2] \exp\left\{\frac{(B_1 - \sqrt{\Delta})^2}{32\alpha}\right\} \times \\ & \left(\operatorname{erf}\left\{\frac{-B_1 + \sqrt{\Delta}}{4\sqrt{2\alpha}}\right\} - 1\right). \end{aligned} \quad (\text{D.16})$$

When we normalize κ and $\overline{C}_{ii} - \delta_{ii}$ in Eq. (62) and substitute the scaling laws for $c_{ij}(x)$ and $u'(x)$ the rheological parameters that appear in the equation cancel out and we obtain the following relation

$$g_{ii}(\xi) = \chi_{c_{ii}} K(\xi)^{3/2} \quad (\text{D.17})$$

where model parameters, such as A_{SDR} , A_ϵ , $A_{c_{ii}}$ and so on, have been absorbed into a single constant coefficient $\chi_{c_{ii}}$, whose value is calculated as described before for the other $\chi_{c_{ij}}$ constants. At the final region of decay we have $g_{xx}(\xi) = -g_{yy}(\xi)$, and so the component $g_{zz}(\xi)$ can be obtained directly from the trace $g_{ii}(\xi)$ i.e.

$$g_{zz}(\xi) = g_{ii}(\xi). \quad (\text{D.18})$$

D.2. Planar jet

The intermittency model used for jets is the same as that described for wakes but $u_{turb}(x, y) = U_c(x)\tilde{\psi}(\xi)$ and $u_{pot} = U_\infty = 0$ for a jet without co-flow. Tollmien (1926) [2] was the first to obtain a solution for $\tilde{\psi}(\xi)$ in a turbulent planar jet, but here we adopt the solution of Görtler (1942) [4], which uses the closure assumption of Eq. (57) and is given by

$$\tilde{\psi}(\xi) = \operatorname{sech}^2(\alpha\xi) \quad (\text{D.19})$$

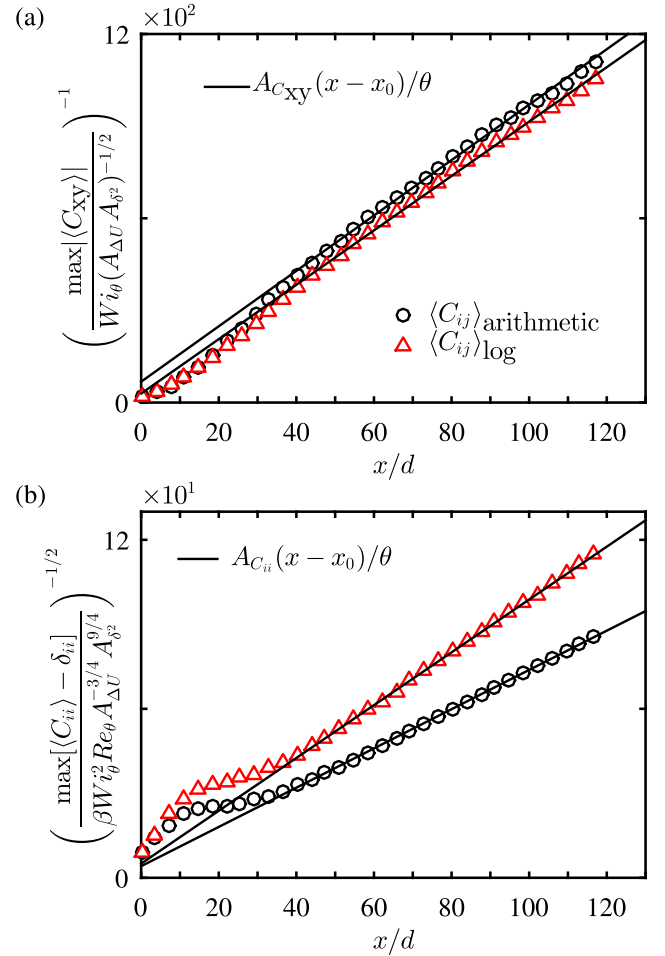


Fig. E.30. Streamwise evolution of normalized $c_{ij}(x)$ compared to the theory for turbulent wakes at the nearly-coiled nearly-isotropic regime: (a) shear component, (b) trace. For each panel, we compute the mean conformation tensor using two different approaches, the classical arithmetic averaging adopted in the core of the manuscript, and the log-Euclidean averaging of Hamenduddin and Zaki (2019) [18]. The DNS parameters are $Re = 3000$, $Wi = 0.15$, $1 - \beta = 0.20$ and $L = 100$.

with $\alpha = \ln[(1 + \sqrt{2})^2]/2$. Combining the above equation with the adopted intermittency model we obtain $\psi(\xi)$, and substitution of the result into Eqs. (37) and (55) leads to the solutions for the normalized conformation tensor components:

$$g_{xy}(\xi) = -\chi_{c_{xy}} \operatorname{sech}^2(\alpha\xi) \times \left\{ \operatorname{tgh}(\alpha\xi) \left[1 - \operatorname{erf}\left(\frac{\xi - \mu}{\sqrt{2}\sigma}\right) \right] + \frac{\exp\left[\frac{-(\xi - \mu)^2}{2\sigma^2}\right]}{\sqrt{2\pi}\sigma} \right\}, \quad (\text{D.20})$$

$$g_{xx}(\xi) = \chi_{c_{xx}} \operatorname{sech}^2(\alpha\xi) \times \left\{ \left[\frac{1}{2} - 2\xi \operatorname{tgh}(\alpha\xi) \right] \left[1 - \operatorname{erf}\left(\frac{\xi - \mu}{\sqrt{2}\sigma}\right) \right] - 2\xi \frac{\exp\left[\frac{-(\xi - \mu)^2}{2\sigma^2}\right]}{\sqrt{2\pi}\sigma} \right\}, \quad (\text{D.21})$$

and again Eq. (D.6) for $g_{yy}(\xi)$.

The linearized differential equation of $K(\xi)$ for the turbulent planar jet is

$$\begin{aligned} & \frac{\tilde{v}_t A_\delta^3}{A_\sigma} \frac{d^2 K}{d\xi^2} + \left(\frac{A_\delta^2}{2} \int_0^\xi \psi d\tilde{\xi}\right) \frac{dK}{d\xi} + \\ & (A_\delta^2 \psi - A_\epsilon A_\delta^3 \sqrt{K_0}) K = -\tilde{v}_t A_\delta^{\frac{1}{2}} \left(\frac{d\psi}{d\xi}\right)^2, \end{aligned} \quad (\text{D.22})$$

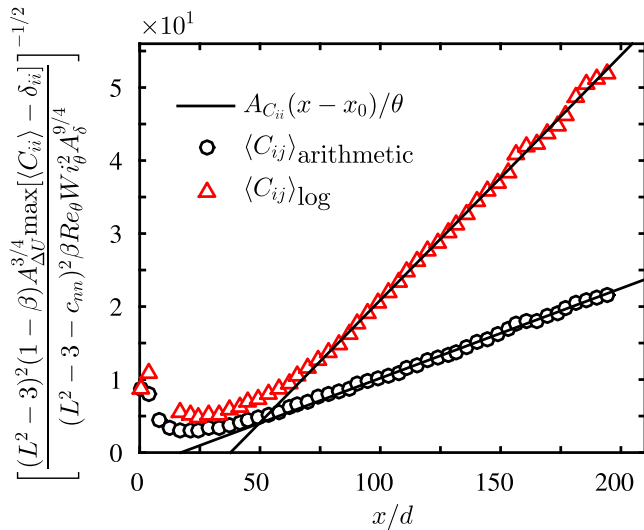


Fig. E.31. Streamwise evolution of normalized $c_{ii}(x)$ compared to the theory for turbulent wakes at the highly-stretched nearly-isotropic regime. The mean conformation tensor is computed using two different approaches, the classical arithmetic averaging adopted in the core of the manuscript, and the log-Euclidean averaging of Hameduddin and Zaki (2019) [18]. The DNS parameters are $Re = 2000$, $Wi = 3$, $1 - \beta = 0.02$ and $L = 200$.

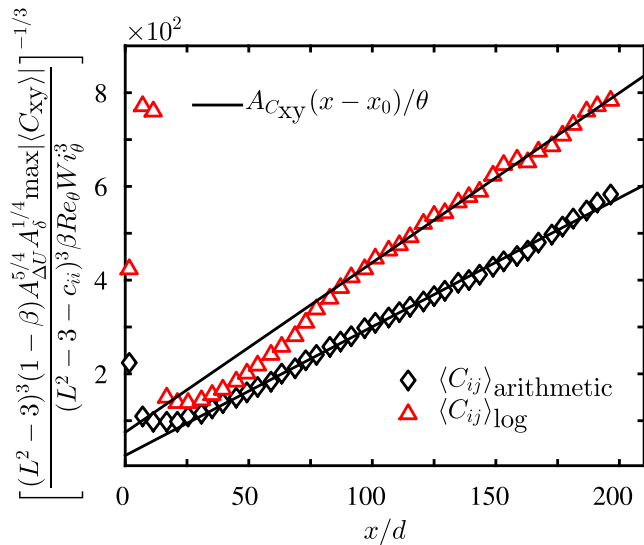


Fig. E.32. Streamwise evolution of normalized $c_{xy}(x)$ compared to the theory for turbulent wakes at the highly-stretched nearly-isotropic regime. The mean conformation tensor is computed using two different approaches, the classical arithmetic averaging adopted in the core of the manuscript, and the log-Euclidean averaging of Hameduddin and Zaki (2019) [18]. The DNS parameters are $Re = 2000$, $Wi = 3$, $1 - \beta = 0.02$ and $L = 200$.

For the jet we were unable to obtain a closed form analytical solution of the ODE, so a numerical solution was presented instead. Subsequently, inserting this numerical solution into Eqs. (D.17) and (D.18) gives the final solutions for $g_{ii}(\xi)$ and $g_{zz}(\xi)$.

Appendix E. Arithmetic and log-Euclidean averages of the conformation tensor

Recently, Hameduddin et al. (2018) [17] and Hameduddin and Zaki (2019) [18] proposed new ways to calculate the mean conformation tensor and its fluctuations that are alternatives to the classical Reynolds decomposition and averaging, namely the log-Euclidean and geometric

means. They argue that their approach is more consistent from both mathematical and physical viewpoints. The log-Euclidean and geometric means behave similarly but the former is more computationally efficient. Here we demonstrate that our new scaling laws derived in the core of the manuscript are also able to describe the evolution of the mean conformation tensor when the log-Euclidean mean is adopted. For brevity, we only show the results from two cases, at highly-stretched and nearly-coiled regimes.

The log-Euclidean mean involves the matrix logarithm and matrix exponential, and is defined by

$$\langle C \rangle_{\log} = \exp(\langle \ln C \rangle_{\text{arithmetic}}), \quad (\text{E.1})$$

where $\langle \cdot \rangle_{\text{arithmetic}}$ indicates the classical arithmetic mean (an over-bar was used in the core of the manuscript).

The trace and shear component of the mean conformation tensor of turbulent wakes, normalized according to our theory, are shown in Fig. E.30 for the nearly-coiled nearly-isotropic regime, and Figs. E.31 and E.32 for the highly-stretched nearly-isotropic regime. In each figure, two methods were used to calculate the mean conformation tensor, the log-Euclidean and arithmetic means. Our analytical scaling laws are also displayed for comparison, and show very good agreement with the DNS data also when the log-Euclidean mean is adopted.

References

- [1] L. Prandtl, 7. Bericht über Untersuchungen zur ausgebildeten Turbulenz, ZAMM 5 (2) (1925) 136–139.
- [2] W. Tollmien, Berechnung turbulenter Ausbreitungsvorgänge, ZAMM 6 (6) (1926) 468–478.
- [3] H. Schlichting, Über das ebene Windschattenproblem, Ing.-Arch. 1 (5) (1930) 533–571.
- [4] H. von Görtler, Berechnung von Aufgaben der freien Turbulenz auf Grund eines neuen Näherungsansatzes, ZAMM 22 (5) (1942) 244–254.
- [5] J.O. Hinze, Turbulence, an Introduction to Its Mechanism and Theory, first ed., McGraw-Hill, 1959.
- [6] A.A. Townsend, The Structure of Turbulent Shear Flow, second ed., Cambridge University Press, Cambridge, 1976.
- [7] H. Tennekes, J.L. Lumley, A First Course in Turbulence, The MIT Press, 1972.
- [8] S.B. Pope, Turbulent Flows, Cambridge University Press, 2000.
- [9] M.C. Guimarães, N. Pimentel, F.T. Pinho, C.B. da Silva, Direct numerical simulations of turbulent viscoelastic jets, J. Fluid Mech. 899 (2020) A11.
- [10] M.C. Guimarães, F.T. Pinho, C.B. da Silva, Turbulent planar wakes of viscoelastic fluids analysed by direct numerical simulations, J. Fluid Mech. 946 (2022) A26.
- [11] J.M. Rallison, E.J. Hinch, Instability of a high-speed submerged elastic jet, J. Fluid Mech. 288 (1995) 311–324.
- [12] P.K. Ray, T.A. Zaki, Absolute/convective instability of planar viscoelastic jets, Phys. Fluids 27 (1) (2015) 014110.
- [13] S. Yamani, B. Keshavarz, Y. Raj, T.A. Zaki, G.H. McKinley, I. Bischofberger, Spectral universality of elastoinertial turbulence, Phys. Rev. Lett. 127 (7) (2021) 074501.
- [14] S. Yamani, Y. Raj, T.A. Zaki, G.H. McKinley, I. Bischofberger, Spatiotemporal signatures of elastoinertial turbulence in viscoelastic planar jets, Phys. Rev. Fluids 8 (6) (2023) 064610.
- [15] M.C. Guimarães, F.T. Pinho, C.B. da Silva, Viscoelastic jet instabilities studied by direct numerical simulations, Phys. Rev. Fluids 8 (10) (2023) 103301.
- [16] M.C. Guimarães, F.T. Pinho, C.B. da Silva, Mixing of passive scalar and polymer concentration in turbulent viscoelastic planar jets and wakes analysed by direct numerical simulations, in: Bulletin of the American Physical Society: 75th Annual Meeting of the Division of Fluid Dynamics, Indianapolis, USA, 2022.
- [17] I. Hameduddin, C. Meneveau, T.A. Zaki, D.F. Gayme, Geometric decomposition of the conformation tensor in viscoelastic turbulence, J. Fluid Mech. 842 (2018) 395–427.
- [18] I. Hameduddin, T.A. Zaki, The mean conformation tensor in viscoelastic turbulence, J. Fluid Mech. 865 (2019) 363–380.
- [19] R.B. Bird, P.J. Dotson, N.L. Johnson, Polymer solution rheology based on a finitely extensible bead-spring chain model, J. Non-Newton. Fluid Mech. 7 (2) (1980) 213–235.
- [20] R. Sureshkumar, A.N. Beris, R.A. Handler, Direct numerical simulation of the turbulent channel flow of a polymer solution, Phys. Fluids 9 (3) (1997) 743–755.
- [21] C. Canuto, M.Y. Hussaini, A. Quarteroni, T.A. Zang, Spectral Methods in Fluid Dynamics, Springer-Verlag, 1987.
- [22] S.K. Lele, Compact finite difference schemes with spectral-like resolution, J. Comput. Phys. 103 (1) (1992) 16–42.
- [23] J.H. Williamson, Low-storage Runge-Kutta schemes, J. Comput. Phys. 35 (1) (1980) 48–56.

- [24] J. Kim, P. Moin, Application of a fractional-step method to incompressible Navier-Stokes equations, *J. Comput. Phys.* 59 (2) (1985) 308–323.
- [25] T. Vaithianathan, A. Robert, J.G. Brasseur, L.R. Collins, An improved algorithm for simulating three-dimensional, viscoelastic turbulence, *J. Non-Newton. Fluid Mech.* 140 (1) (2006) 3–22.
- [26] A. Kurganov, E. Tadmor, New high-resolution central schemes for nonlinear conservation laws and convection-diffusion equations, *J. Comput. Phys.* 160 (1) (2000) 241–282.
- [27] F. Pinho, C. Li, B. Younis, R. Sureshkumar, A low Reynolds number turbulence closure for viscoelastic fluids, *J. Non-Newton. Fluid Mech.* 154 (2–3) (2008) 89–108.
- [28] P.C. Valente, C.B. da Silva, F.T. Pinho, The effect of viscoelasticity on the turbulent kinetic energy cascade, *J. Fluid Mech.* 760 (2014) 39–62.
- [29] P.C. Valente, C.B. da Silva, F.T. Pinho, Energy spectra in elasto-inertial turbulence, *Phys. Fluids* 28 (7) (2016) 075108.
- [30] F.C. Li, W.H. Cai, H.N. Zhang, Y. Wang, Influence of polymer additives on turbulent energy cascading in forced homogeneous isotropic turbulence studied by direct numerical simulations, *Chin. Phys. B* 21 (11) (2012) 114701.
- [31] M.Q. Nguyen, A. Delache, S. Simoëns, W.J.T. Bos, M. El Hajem, Small scale dynamics of isotropic viscoelastic turbulence, *Phys. Rev. Fluids* 1 (8) (2016) 083301.
- [32] R.C. Armstrong, Kinetic theory and rheology of dilute solutions of flexible macromolecules. I. Steady state behavior, *J. Chem. Phys.* 60 (3) (1974) 724–728.
- [33] A.J. Sarnecki, *The Turbulent Boundary Layer on a Permeable Surface* (Ph.D. thesis), Cambridge University, 1959.
- [34] D. Krug, J. Philip, I. Marusic, Revisiting the law of the wake in wall turbulence, *J. Fluid Mech.* 811 (2017) 421–435.
- [35] M.C. Guimarães, D.O.A. Cruz, A.P. Silva Freire, Similarity laws for transpired turbulent flows subjected to pressure gradients, separation and wall heat transfer, *Int. J. Heat Fluid Flow* 78 (2019) 108436.
- [36] K.N.C. Bray, P.A. Libby, J.B. Moss, Unified modelling approach for premixed turbulent combustion Part 1: General formulation, *Combust. Flame* 61 (1) (1985) 87–102.
- [37] L. Prandtl, *Über Ein Neues Formelsystem Für Die Ausgebildete Turbulenz*, Vandenhoeck and Ruprecht, 1945.
- [38] D.C. Wilcox, *Turbulence Modeling for CFD*, third ed., DCW Industries, 2006.
- [39] S. Corrsin, A.L. Kistler, Free-stream boundaries of turbulent flows, Technical Report 1244, National Advisory Committee for Aeronautics, 1955.
- [40] P.S. Klebanoff, Characteristics of Turbulence in a Boundary Layer with Zero Pressure Gradient, Technical Report 1247, National Advisory Committee for Aeronautics, 1955.